1999 NSREC

SHORT COURSE

SECTION IVB

PROTON EFFECTS AND TEST ISSUES FOR SATELLITE DESIGNERS: DISPLACEMENT EFFECTS

Cheryl J. Marshall
NASA/Goddard Space Flight Center

Paul W. Marshall
Consultant

IV. Proton Effects and Test Issues for Satellite Designers

Part B: Displacement Effects

Cheryl J. Marshall
NASA/Goddard Space Flight Center
Electrical Systems Center / Code 562
Greenbelt, Maryland 20771

Paul W. Marshall
Consultant
7655 Hat Creek Road
Brookneal, VA 24528

1.0 INTRODUCTION

Microelectronic and photonic systems in the natural space environment are bombarded by a variety of charged particles including electrons, trapped protons, cosmic rays, and solar particles (protons and other heavy ions). These incident particles cause both ionizing and non-ionizing effects when traversing a device, and the effects can be either transient or permanent. The vast majority of the kinetic energy of an incident proton is lost to ionization, creating the single event effects (SEEs) and total ionizing dose (TID) effects described in section IVA. However, the small portion of energy lost in non-ionizing processes causes atoms to be removed from their lattice sites and form permanent electrically active defects in semiconductor materials. These defects, i.e., "displacement damage," can significantly degrade device performance. In general, most of the displacement damage effects in the natural space environment can be attributed to protons since they are plentiful and extremely energetic (and therefore not readily shielded against). For this reason, we consider only proton induced displacement damage in this course. (Nevertheless, we identify solar cells as an important example of a case where both electron and proton damage can be important since only very light shielding is feasible.) The interested reader is encouraged to explore the three previous NSREC and RADECS short courses [Srou88a, Summ92, Hopk97] which also treat displacement damage issues for satellite applications. Part A of this segment of the short course introduces the space environment, proton shielding issues, and requirements specifications for proton-rich environments. In order to exercise the displacement damage analysis tools for on-orbit performance predictions, the requirements document must provide the relevant proton spectra in addition to the usual total ionizing dose-depth curves.

Ion-solid interactions and the nature of the displacement damage they generate have been studied extensively for over half a century, yet they still remain a subject of investigation. In this section, a description of the mechanisms by which displacement damage is produced will be followed by a summary of the major consequences for device performance in a space environment. Often the degradation of a device parameter can be characterized by a damage factor (measured in a laboratory using monoenergetic protons) that is simply the change in a particular electrical or optical parameter per unit proton fluence. In addition, we will describe the concept of a non-ionizing energy loss rate (NIEL) which quantifies that portion of the energy lost by an incident ion that goes into displacements. It has been calculated as a function of proton energy, and is analogous to (and has the same units as) the linear energy transfer (LET) for ionizing energy. We will discover that, to first order, the calculated NIEL describes the energy dependence of the measured device damage factors. This observation provides the basis for predicting proton induced device degradation in a space environment based on both the calculated NIEL and relatively few laboratory test measurements. The methodology of such on-orbit device performance predictions will be described, as well as the limitations.

Several classes of devices for which displacement damage is a significant (if not the dominant) mode of radiation induced degradation will be presented. The examples

will illustrate various aspects of displacement damage in more detail. We will see, over and over, that the impact of a particular level of damage on device performance is very application-dependent. It will also become clear that uncertainties in the on-orbit prediction for devices sensitive to displacement damage may require significantly increased radiation design margins. All too often, the design engineer is more familiar with basic total ionizing dose (TID) and traditional SEE effects, and may find it difficult to accept the need for proton testing, and especially, any increased radiation design margin associated with uncertainties in displacement damage analyses. There is an increasing demand to employ displacement damage sensitive devices (e.g., charge coupled devices (CCDs), photodetectors, light emitting diodes (LEDs), optocouplers, solar cells, and high precision linear devices) in harsh proton environments (and/or on longer missions). This has led to a renewed interest in hardness assurance techniques for such devices [LaBe98]. It is hoped that this course will provide the understanding necessary for a radiation effects engineer to identify technologies requiring evaluation for possible displacement effects, use the current literature to make first order estimates of device performance, and help ensure that appropriate laboratory radiation testing and analyses are performed. *For those readers interested in surveying proton induced device effects (as opposed to performing displacement damage analyses), we recommend reading section 2.2 on displacement effects in devices followed by section 3.3 which includes case studies of those technologies most affected by displacement damage.*

2.0 PROTON INDUCED DISPLACEMENT DAMAGE MECHANISMS AND TOOLS

In this section, we describe proton displacement effects, on-orbit prediction tools for device performance and laboratory radiation test issues. We begin with a general description of the underlying physical processes that generate displacement damage. The initial production of defects in the semiconductor by incident protons, and the subsequent evolution of this damage to its final stable defect configuration is then described in section 2.1. We discuss the processes by which these defects electrically alter the semiconductor material, and thereby impact device performance in section 2.2. Section 2.3 contains a description of the non-ionizing energy loss rate (NIEL), after which we present the first order correlation between NIEL and device degradation that is experimentally observed. We identify the implications of this correlation in terms of the basic damage mechanisms described in section 2.1, and provide the basis for understanding the limitations of the correlation in section 2.3.2.

The NIEL concept enables comparison of the displacement damage produced by protons of different energies (or a spectrum of proton energies) via the calculation of displacement damage equivalent fluences (section 2.3.3), or the "displacement damage dose" (section 2.3.4). This is analogous to the calculation of total ionizing dose based on the proton fluence and LET [see section IVA, equation 1]. Using these tools we establish a methodology for on-orbit device performance predictions in section 2.4. Figure 1 summarizes the method used to predict the on-orbit device (or circuit) response to

displacement damage. Note that some devices may have significant concurrent total ionizing dose effects that must also be considered.

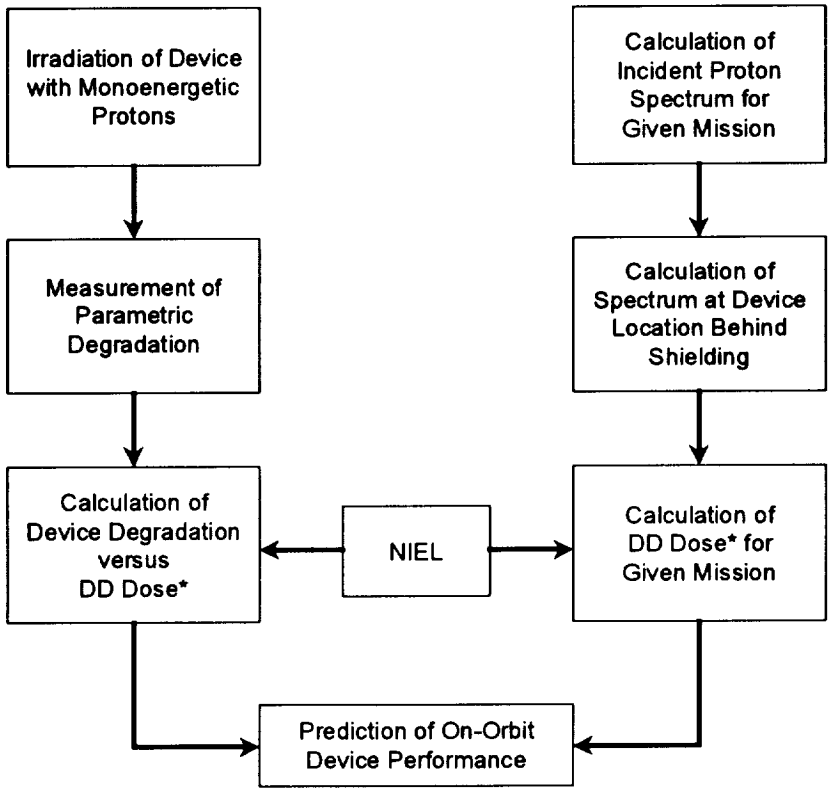

Figure 1 Block diagram of the generic methodology for performing a on-orbit predictions of device performance when device degradation is dominated by displacement damage effects.

2.1 Displacement Damage Mechanisms and Defect Formation

As indicated above, the interaction between a charged particle (such as a proton) and a solid cause both ionizing and non-ionizing effects. Most of the kinetic energy of an incident proton is lost in interactions with atoms in the semiconductor that transfer energy to the electron clouds causing excitation or ionization. However, a very small fraction (< 0.1%) of the energy loss causes the atoms to be displaced from their equilibrium sites, and can lead to lattice disorder. An incident proton may collide with a semiconductor nucleus and displace it from its site producing a primary knock-on atom (PKA). If sufficiently energetic, the PKA displaces more atoms, and the collision cascade proceeds until the magnitude of energy transferred becomes less than the threshold required for displacements. At a given incident proton energy, the recoil atoms can vary in kinetic energy from near zero up to some maximum determined by collision mechanisms. Both

the average recoil energy and the shape of the recoil spectrum depend on the energy, mass, and charge of the incident particle and the mass of the target.

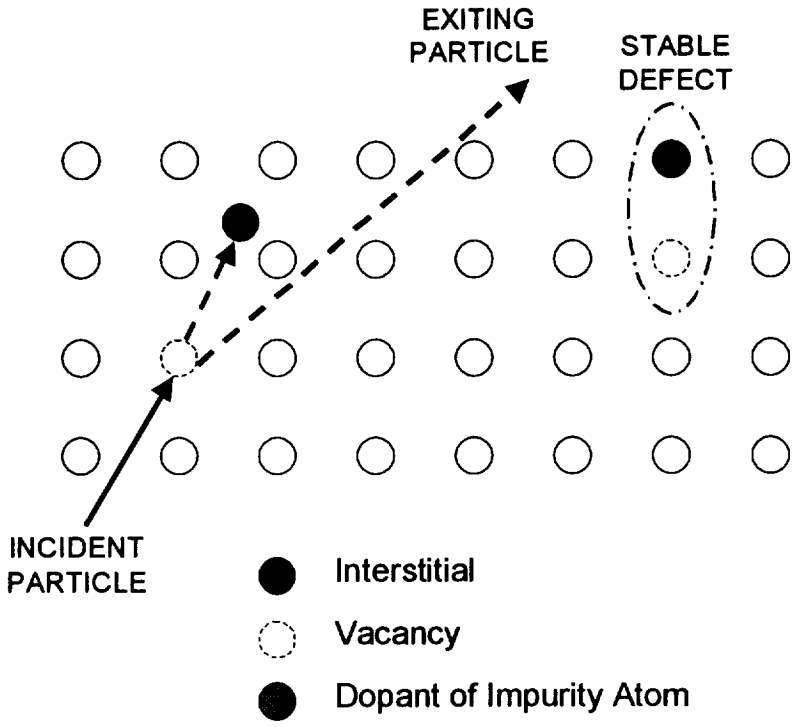

Figure 2a Cartoon showing the displacement of an atom from its lattice site by an incoming proton, thereby forming a vacancy-interstitial (Frenkel) pair. Surviving vacancies migrate through the lattice and often form electrically active stable defects in conjunction with an impurity or dopant atom.

Regardless of whether an atom is displaced as a part of a damage cascade or as an isolated lower energy PKA, most of the initial vacancy-interstitial pairs recombine and no permanent damage results. The interstitial Si atoms do not form electrically active defects. However, the vacancies that escape recombination migrate through the lattice and ultimately form relatively long-lived and immobile defects. Figure 2a is a cartoon illustrating how the initial formation of a Frenkel pair, which is unstable, ultimately results in the formation of a stable defect. These defects have energy levels within the bandgap of the semiconductor. For example, in Si, two vacancies may combine to form a divacancy that is stable up to about 300 °C, or a vacancy and a phosphorous (or oxygen) atom may form an E center (or A center) which is stable up to about 150 °C (or 350 °C), respectively [e.g., Watk64, Walk73 and Kime79]. The vacancy itself is mobile even at liquid nitrogen temperatures, so it is not practical to attempt to prevent the formation of these defects. The process during which the initial vacancy-interstitial pairs evolve into stable room temperature defects results in the so-called "short term annealing effects" in Si devices, and is usually complete within about a second [Srou70, Hein83, Gove84, Mess86]. Figure 2b is a qualitative pictorial showing the time evolution of the number of surviving defects. Note that the stable damage produced in a space environment is very dilute. Longer term room temperature annealing is often observed over a period of

days or weeks, but it is generally a small effect. For this reason, displacement damage is considered to be a "permanent effect."

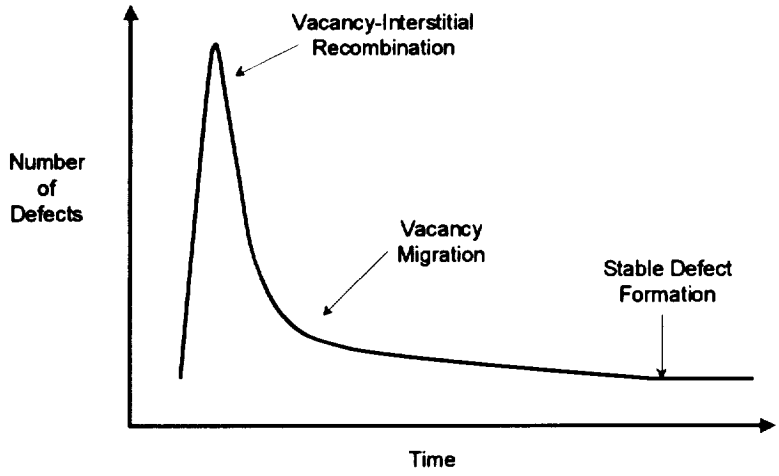

Figure 2b Illustration the time evolution of the initial vacancy-interstitial pairs to the formation of stable defects. The annealing of Frenkel defects occurs in less than 1 millisecond and stable defects are formed on the time scale of seconds.

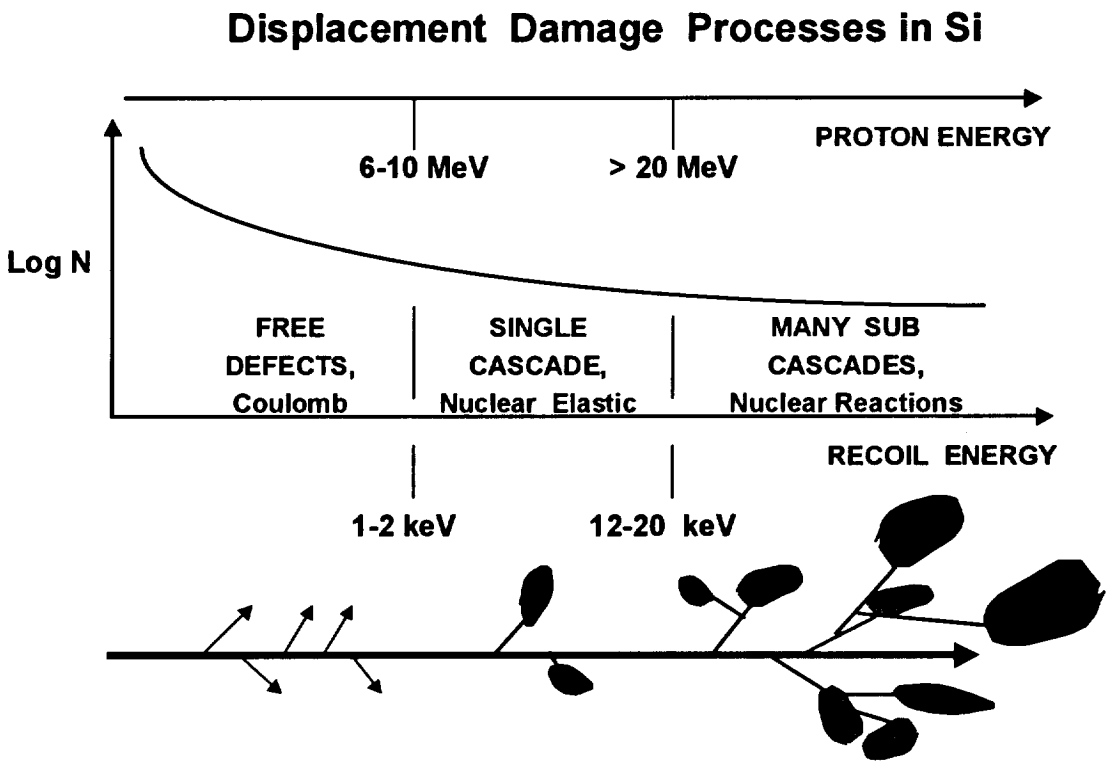

Figure 3 Pictorial relating the initial defect configuration to the primary knock-on atom (PKA) energy in Si material. Note from the plot of the number of interactions (N) versus incident proton energy that most interactions are Coulomb events producing isolated defects. For recoil energies

above a couple of keV, the overall damage structure is relatively unchanged due to the formation of cascades and subcascades. After [Wood81].

The final configuration of electrically active defects formed by particle irradiation has been a topic of much research, but is still not well understood. As we will see this issue is at the heart of understanding the use and limitations of calculated non-ionizing energy loss rate (NIEL) damage functions to predict the displacement damage response of a device in a proton environment. Figure 3 is a pictorial of the spatial distribution of the *initial* vacancy-interstitial pairs in Si investigated using the Monte Carlo code MARLOWE [More82]. As can be seen from the plot of the log of the number of interactions (Log N) versus the incident proton energy, most events are Coulomb interactions which produce PKAs with $E_{threshold} < E < \sim 2$ keV, and result in isolated defects. Although there are many fewer of the nuclear elastic and inelastic reaction events that produce cascades, these events are far more damaging, and can contribute a significant fraction of the total displacement damage at higher proton energies. As indicated in the figure, recoils with energies between about 2-10 keV produce single subcascades, whereas those with energies in excess of 12-20 keV form a tree-like structure with branches containing multiple subcascades.

Similar results were obtained for Si by Mueller et al. who also investigated the defect structure near the end of the recoil track. The term "terminal cluster" has been used to describe the damaged region where the recoil ion loses the last 5-10 keV of energy and has the highest elastic scattering cross section [Muel82]. They found that a single cascade is likely to have 2-3 terminal clusters with a characteristic dimension of 5 nm, connected to each other by a string of dilute displacements. (Note that this size is an upper limit since the calculation does not include the initial vacancy-interstitial recombination.) This result is consistent with transmission electron microscopy measurements [Lars78, Nara81] of 1 MeV, 14 MeV and fission neutron-irradiated Si that have found an average size of 4 nm for the damage. It is clear that the early terminal cluster models based on heavily damaged regions extending for 200 nm [VanL80, and references therein] are not supported by more recent work. Unfortunately, the early cluster models derived support from electron microscopy [Bert68] work that later was shown to be compromised by faulty etching techniques [Nara88]. We also note that electrical measurements on irradiated devices performed in the last decade or so are also inconsistent with the early cluster models. The interested reader may refer to the literature for details [e.g., Summ87, Peas87, Dale88].

2.2 Displacement Damage Effects in Materials and Devices

The net electrical activity of a given defect with an energy level (E_t) in the bandgap is ultimately produced by five basic processes as illustrated in figure 4: (1) the generation of electron-hole pairs, (2) the recombination of electron-hole pairs, (3) carrier trapping, (4) the compensation of donors or acceptors, and (5) the tunneling of carriers.

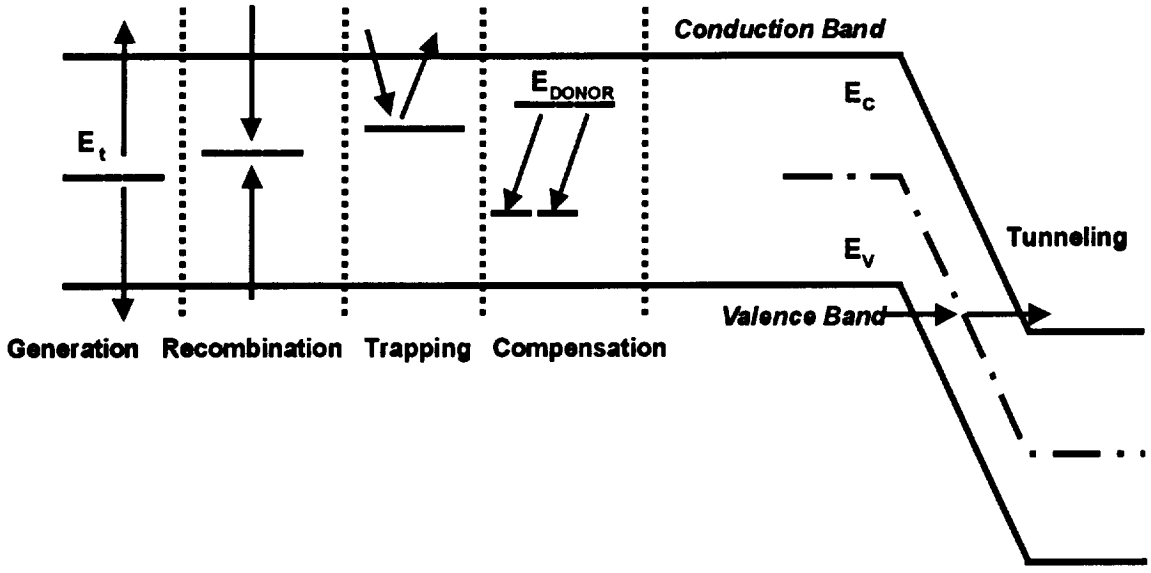

Figure 4 Schematic of the electrical effects that may occur due to the presence of radiation induced defect levels in the band gap of a semiconductor. After [Gove84].

Physically, *electron-hole pair generation* occurs by the thermal excitation of an electron from the valance band to the defect level followed by its emission to the conduction band. Midgap energy levels in a depletion region are most effective at generating dark current in a device via this process. *Recombination* occurs when a carrier of one sign is captured at a defect, and not re-emitted before a carrier of the opposite sign is also captured. The energy may be released in the form of light (radiative recombination), or in the form of phonons (i.e., lattice vibrations) which is termed non-radiative recombination. The minority carrier lifetime, which is a key parameter in device performance, is determined by the recombination rate [e.g., Schr82]. *Carrier trapping* refers to the process whereby a carrier is captured at a defect and then released to its original band. In the case of CCDs, signal charge may be trapped only to be released after the signal packet has already passed causing the charge transfer efficiency of the device to degrade [Mohs74]. Filled traps with a net charge are more effective scattering centers thereby reducing carrier mobility. Carrier removal results when a majority carrier is trapped. *Compensation* is also responsible for carrier removal. As seen in the figure (for n-type material), the free electrons provided by the shallow donor levels are compensated by deep lying acceptor levels thereby reducing the net carrier concentration. For example, the resistance in a lightly doped collector of a bipolar transistor can increase as a result of this type of carrier removal. Finally, *defect levels can assist tunneling through a potential barrier* in the bandgap. This effect can produce increased current in a reverse biased junction, and is most significant in materials with small bandgaps and high electric fields.

The most important material parameters for the practical operation of most semiconductor devices are the minority carrier lifetime, the generation lifetime [Schr82], the majority carrier concentration and the majority carrier mobility. Typically, the semiconductor material quality is high so that there is at least an order of magnitude smaller density of recombination and generation centers as compared to the majority carrier concentration. As a result, the proton induced introduction of defects (i.e., recombination centers) will impact the minority carrier lifetime well before there is a noticeable reduction in carrier concentration. The same is true for defects produced in depletion regions that can act to decrease the generation lifetime. Mobility degradation is not generally an issue except at very high displacement damage levels. Hence, devices whose primary characteristics depend on minority carrier or generation lifetimes will be most sensitive to displacement damage.

Radiation induced degradation in the carrier lifetime, carrier concentration and mobility in turn impact device characteristics such as transistor gain, transconductance and saturation voltage, dark current, detector responsivity, etc. As just described, the reduction of the minority carrier lifetime is a principal cause of degradation in a number of device types. Examples include gain reduction in bipolar transistors and silicon controlled rectifiers (SCRs), reduced responsivity in photodiodes and Schottky-barrier diodes, decreased solar cell efficiency, etc. Devices with lightly doped active regions are most susceptible to degradation caused by carrier removal. Semiconductor light sources such as lasers and LEDs are generally relatively radiation hard since the carrier lifetimes in the active device regions are very short. However, amphoterically-doped LEDs, employed in some optocouplers, are a notable exception and are quite sensitive to proton induced displacement damage for reasons that are not completely understood.

Displacement damage effects do not limit the performance of most MOS devices, which depend on majority carrier transport. Exceptions include optoelectronic device types such as the charge injection device (CID) and charge coupled device (CCD), which are extremely sensitive to displacement damage. CCDs are subject to dark current increases resulting from decreased generation lifetime, and from charge transfer efficiency (CTE) degradation due to carrier trapping. JFET and MESFET technologies, being majority carrier devices, are generally very robust to displacement damage [e.g., Hash94] although their transconductance may be degraded by carrier removal at high proton exposure levels. Table 1 summarizes the relative importance (primary or secondary) of displacement damage in many common device technologies [after Srou88a].

Radiation effects experience over the last 20 years has led to a general understanding of device type sensitivities and degradation modes in response to displacement damage. Summaries of these efforts may be found in general radiation effects texts [e.g., Mess86, Holm93] and in a number of summary papers [e.g., Gove84, Srou88b, Raym87]. The case studies to be considered in this course will also provide brief descriptions of displacement damage effects in selected device types.

Table 1. Displacement Damage Mechanisms for Various Technologies[1]

Component	Lifetime Degradation	Carrier Removal	Trapping	Mobility Degradation
Si MOS Transistors & ICs				S
Charged Coupled Devices	P		P	
Si Bipolar Transistors & Linear ICs	P	S		
Photodetectors	P			
LEDs & Laser Diodes	P			
pn Junctions	P	P	P	
JFETs		P	P	S
GaAs Transistors & ICs		P		S

P = Primary; S = Secondary

[1]After [Srou88a]. Note that TID and SEEs also can be primary radiation concerns for these technologies.

2.3 Non-Ionizing Energy Loss Rate (NIEL) Concept

As we will see in the next section, it has been shown that the radiation response of many devices can be predicted reasonably well based on calculations of the amount of displacement damage energy imparted to the primary knock-on atoms. The non-ionizing energy loss rate (NIEL) can be calculated analytically from first principles based on differential cross sections and interaction kinematics. NIEL is that part of the energy introduced via both Coulomb (elastic), nuclear elastic, and nuclear inelastic interactions, which produces the initial vacancy-interstitial pairs and phonons (e.g., vibrational energy). NIEL can be calculated using the following analytic expression that sums the elastic and inelastic contributions as:

$$\mathrm{NIEL} = (N/A)\,[\sigma_e T_e + \sigma_i T_i]. \qquad (1)$$

The σ's are total cross sections, the T's are effective average recoil energies corrected for ionization loss using the Lindhard theory [Lind63], N is Avogadro's number, and A is the gram atomic weight of the target material. In the case of compounds, the total NIEL is derived as a superposition (weighted by mole fraction) of the contributions for each atomic component [Zeig84]. Notice that the units of NIEL, (keVcm^2/g), are the same as

those for stopping power (or LET) describing energy transfer by ionization and excitation per unit length. Burke has calculated NIEL in silicon for protons and other ions over a broad energy range [Burk86]. More recent calculations by Burke have incorporated improvements in the treatment of the nuclear elastic and inelastic reactions, and the Lindhard correction has been applied to the differential recoil spectrum instead of to the average recoil energy of the target atoms. The more accurate calculation is given by

$$NIEL = N/A \int L[T(\Theta)]T(\Theta)[d\sigma/d\Omega]d\Omega \qquad (2)$$

where $d\sigma/d\Omega$ is the differential cross section for a recoil in direction Θ, $T(\Theta)$ is the recoil energy, and $L[T(\Theta)]$ is the fraction of the recoil energy that goes into displacements [Lind63]. In the case of Si, the maximum amount of displacement damage energy is about 300 keV, regardless of the energy of the recoiling atom. The maximum damage energy increases with atomic number, and is about 2 MeV for GaAs. Figure 5 shows both the LET and NIEL for Si as a function of incident proton energy. Burke has calculated the proton NIEL for a variety of other materials. The most recent published NIEL calculations can be found in the December IEEE Transactions of Nuclear Science cited as follows: InGaAs [Mars92], GaAs and InP [Summ93], and Si [Dale94].

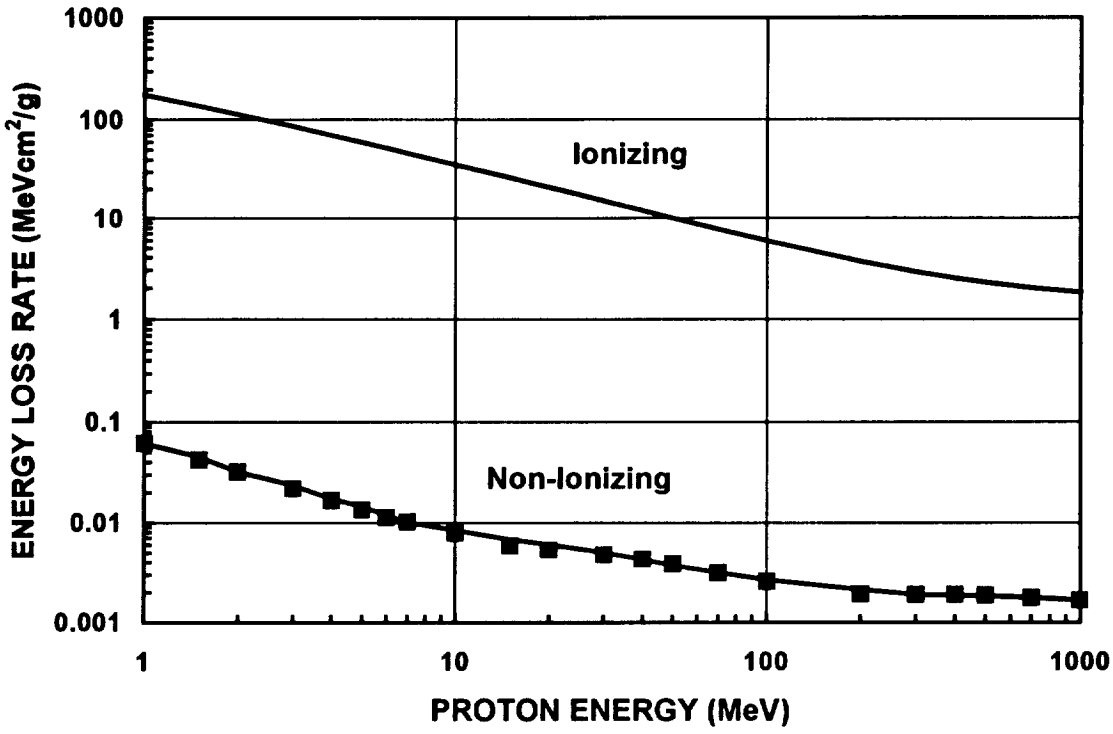

Figure 5 Comparison of the energy loss rate through ionization and excitation of the Si lattice (LET), and through atomic displacements (NIEL) over a wide range of proton energies. The LET was calculated as in [Zeig85], and NIEL as in [Dale94].

The nature of displacement damage as a function of proton energy is governed by the interaction cross sections, and the non-ionizing energy of the PKAs as governed by the Lindhard function. For proton energies below about 10 MeV, Coulomb elastic scattering is by far dominant in Si, and produces atomic recoils with non-ionizing energies in the hundreds of eV. At higher energies, the bend in the curve occurs because nuclear elastic scattering becomes more important resulting in recoils with non-ionizing energies in the tenths of MeV range. As the incident proton energy increases the elastic cross section decreases athough it is still larger than the inelastic cross section. By about 100 MeV half of the non-ionizing energy imparted to the Si lattice is from nuclear inelastic reactions with a mean PKA non-ionizing energy that is still about 0.1 MeV (due to the Lindhard partition).

NIEL has also been calculated by other means including Monte Carlo programs such as HETC [Alur91], CUPID [McNu81, McNu94] and TRIM [Zeig84]. A comparison between the most recent Burke and CUPID calculations of Si NIEL is discussed in [Dale94]. Although HETC, CUPID and Burke's calculations of the recoil distributions as a function of incident proton energy show similar trends, they differ in details [Dale94]. The TRIM program only includes the Coulombic interactions, so it is not appropriate to use it directly for damage calculations for proton energies above about 8 MeV or so, depending on the target material.

Note that all of the above calculations include a "fudge factor" that accounts for the fact the most of the initially produced vacancy-interstitial pairs recombine and therefore do not produce electrically active defects. For example TRIM is often executed assuming a displacement energy threshold of 25 eV, which is considerably higher than the actual value. This practice helps to account for the efficiency of the initial recombination of the vacancy-interstitial pairs. In other Monte Carlo codes such as MARLOWE, one also has the option to define a radius around each collision point for which all the vacancy-interstitial pairs recombine. In essence, all current NIEL calculations must be scaled to fit the experimental damage factors, unless damage factor ratios are compared. As we shall see, it is the calculation of the energy dependence that is relevant, not the absolute values of NIEL.

2.3.1 The Correlation of NIEL to Device Behavior

Device degradation in a radiation environment is often characterized by defining a damage constant, or a damage factor. Damage constants describe the change in basic material parameters such as minority carrier lifetime or diffusion lengths, produced by a given fluence of protons of a specific energy. (Fluence is defined as the number of incident particles per unit target area, and has units of cm^{-2}.) Damage factors are similar except they characterize the observed radiation induced degradation of device or system parameters that may not be readily reduced to basic material parameters because a detailed device model is not available.

The following well known equation describes the degradation in minority carrier devices that results from the reduction in the diffusion length that accompanies the introduction of radiation induced defect recombination centers:

$$1/L^2=1/L_o^2 + K\Phi. \quad (3)$$

The initial and post-radiation diffusion length is given by L_0 and L, respectively, K is the damage constant, and Φ is the proton fluence. (Sometimes this equation appears in terms of the minority carrier lifetime, τ, using the relation, $L = (D\tau)^{0.5}$, where D is the diffusion coefficient.)

Usually the satellite designer or test engineer is interested in a particular device parameter, and defines a relevant damage factor. In the case studies to follow, we will see examples of other useful device damage factors such as the CCD CTE damage factor, the dark current damage factor, the solar cell efficiency damage factor, and so on. In each case, the device parameter in question changes linearly with fluence, or else is defined in the linear region. Note that parameters such as inverse bipolar transistor gain, detector responsivity, and CCD dark current, which have a well-defined regime with a linear response, may also exhibit a nonlinear response at very low or very high proton fluences. (We will also see examples where a device parameter of interest such as LED light output or optocoupler current transfer ratio does *not* behave linearly in the proton fluence regime of interest.)

Bipolar transistor gain measurements for a variety of incident particles (as a function of energy) have been performed in order to determine whether the NIEL function can be used both to predict the energy dependence of the device damage factor and to correlate the degradation due to different particles [Summ87]. In principle, such a correlation also provides the basis for on-orbit performance predictions based on the measurement of a damage factor at a single proton energy. Likewise, if neutron data already exists, the correlation can be used to predict the device response to protons. In this work, the well-known Messenger-Spratt equation is used to describe the radiation response of the common emitter DC gain, h_{FE}, of a bipolar transistor:

$$1/h_{FE} = 1/h_{FEO} + K(E)\Phi \quad (4)$$

where $1/h_{FEO}$ is the initial reciprocal gain, K(E) is the particle and energy dependent displacement damage factor, and Φ is the incident particle fluence. The transistor gain (given by the ratio of the collector to base currents) decreases with increasing proton fluence primarily as a result of the decreased minority carrier lifetime in the base region. A more detailed description may be found in [Mess86]. The damage factor is determined experimentally by performing device gain measurements (for a particular set of device operating conditions) after incremental exposures at a given proton energy.

Figure 6 shows the measured damage factors for protons, deuterons and helium ions normalized to the 1 MeV-equivalent (Si) neutron damage factors as a function of ion energy for a variety of Si bipolar transistors. (We will discuss the meaning of MeV equivalence in a later section, and neutron damage equivalence is explored in [Luer87]. For the present purposes we note that by comparing ratios of measured damage factor to

the calculated NIEL ratios, no scaling parameter is needed to match data with theory.) The importance of this result is the proportionality between the measured damage factors and calculated NIEL that provides the basis of the on-orbit predictions of device degradation produced by displacements.

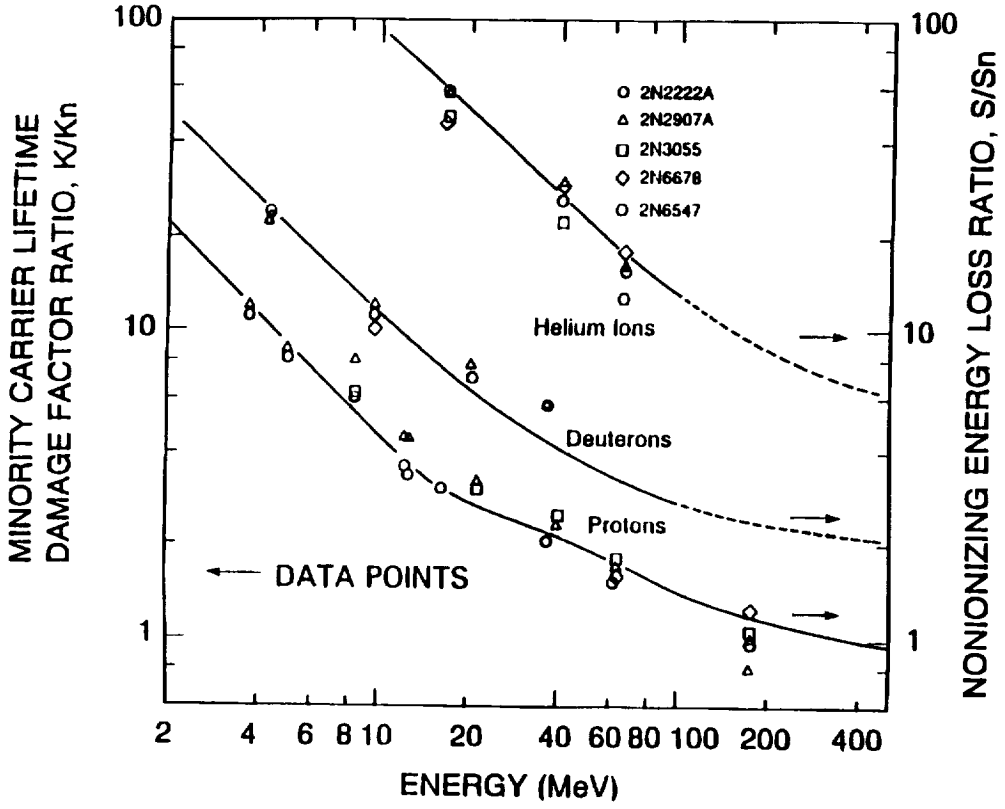

Figure 6 The transistor damage factor ratios for a variety of particles with fission neutrons are shown together with the corresponding calculations of the NIEL ratios. Note that both ordinates are identical (with no fitted parameters), which indicates a direct proportionality between NIEL and the damage factors over a wide energy range. After [Summ87].

Research performed in the last dozen years has shown that, to first order, the linear relationship between the device degradation from particle-induced displacement damage and NIEL holds for a variety of electrical parameters, incident particles, and device materials [Summ87, Peas87, Dale88, Mars89a, Walt91, Mars92, Ohya96, etc.]. This is a surprising result when we consider that NIEL calculations describe the energy deposited into the formation of Frenkel pairs (over 90% of which recombine), and do not consider the process by which the stable electrically active defects are formed. Since NIEL is a direct measure of the initial number of vacancy-interstitial pairs created, the implications of the NIEL correlation with device degradation are that: (1) the percentage of initial vacancy-interstitial pairs that survive recombination is independent of the PKA energy, and (2) the resulting stable defects have the same device effect regardless of whether they evolved from a vacancy-interstitial pair originating in a subcascade or as a well-separated pair [Dale88]. In addition, given that various stable defects have quite

different electrical properties, the correlation also implies that the defect inventory produced is independent of PKA spectrum. Nevertheless, the degree to which the NIEL correlation holds is qualitatively consistent with the Monte Carlo calculations described earlier. These simulations show that a higher energy PKA will produce more overall damage, but that the microscopic nature of the damage is not drastically different. The branching process simply creates more and more subcascades, each separated by a string of relatively isolated defects.

It is still important to keep in mind that, although defects produced from isolated vacancy-interstitial pairs (such as those produced by gamma rays and 1 MeV electrons) may have similar electrical characteristics to those produced by heavier particles such as protons and neutrons, there *are* important differences. These differences are not restricted to short term annealing effects, and also manifest themselves in the long term behavior of a device. For example, E-centers (vacancy-phosphorus defects) produced by 1 MeV electrons anneal at a significantly lower temperature than those produced by protons [Walk73, Kime79], a relevant (and unfortunate) fact for charge coupled device (CCD) engineers who have considered on-orbit warm-ups to mitigate charge transfer efficiency degradation in CCDs [Holl91a]. Differences in the operation of SiGe transistors [Rold98] and AlGaAs/GaAs solar cells [Barn84] have been attributed to differences in the defects produced by neutrons versus protons. Very well controlled deep level transient spectroscopy studies [Eise92, Mind76] have unequivocally demonstrated that, although 1 MeV electrons and protons produce some of the same defects in n-GaAs, there are also different defects produced by each particle. The bottom line for the satellite designer working a mission in a proton environment is that devices that are highly sensitive to displacement damage should be radiation tested with protons. We will see other reasons for this recommendation later in the short course.

2.3.2 Limitations in Usage of NIEL

The NIEL calculation is a useful tool to approximate the expected proton induced radiation response in a space environment, but it is necessary to appreciate the underlying assumptions and limitations in order to use it effectively. Deviations at very low proton energies (approaching the displacement energy thresholds) are expected [Dale 88, Summ93], but they are not generally of concern for *proton* applications in space because they contribute little to the total displacement damage behind typical shielding, as will be shown in section 2.4. However, indications of other systematic deviations from the NIEL correlation have been observed in Si device measurements (e.g., for several CCDs, a CID, a 2N2907 bipolar transistor [Dale88]), and also in GaAs measurements (e.g., an LED [Barr95], a laser diode [Zhao97], solar cells [Walt99], and a JFET [Summ88]). Depending on how the damage factor measurements were normalized to NIEL, the deviations have been reported either as the damage factors being over-estimated by NIEL at higher energies, or equivalently, being underestimated by NIEL at the lower energies. The choice of a damage function (i.e., the energy dependence given by the calculated NIEL or experimental damage factors) has been shown to be significant. For example, one study found a factor of two difference in the on-orbit predictions of the degradation in Si CCD performance depending on which damage function is employed [Dale91].

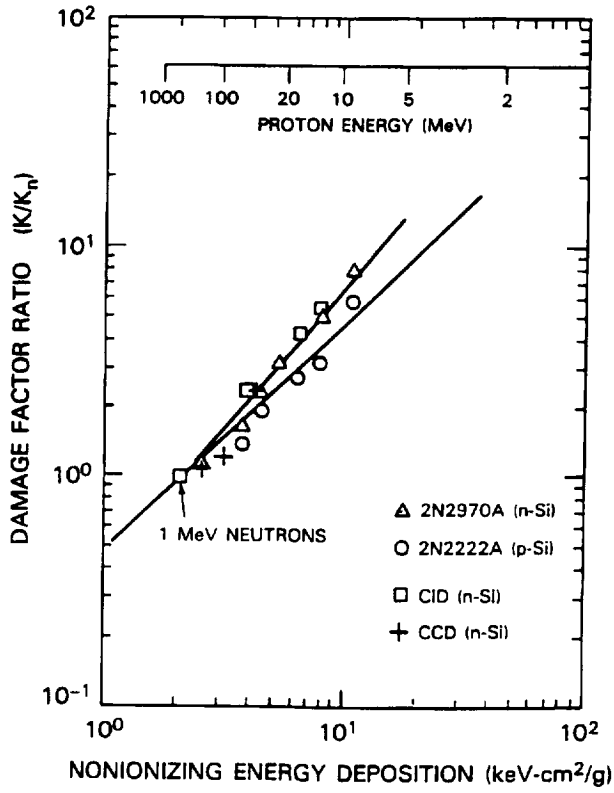

Figure 7 Transistor damage factors and dark current damage factors for protons (normalized to fission neutron damage factors) versus NIEL. The lower line (with a slope of one) indicates a linear relationship between the damage factor ratios and NIEL. The deviations from linearity are indicated with the upper line. [After Dale89b]. A similar figure in [Dale88] also shows deviations for transistor damage factors measured for electrons.

Deviations from the linear dependence of Si displacement damage factors with the NIEL energy dependence are shown in figure 7, which shows the proton to neutron damage factor ratios for several devices plotted as a function of NIEL [Dale88]. The damage factors represent changes in the minority carrier lifetime in the case of the transistor data, and the generation lifetime in the case of the CID and CCD dark current damage factors. A slope of one on the log-log plot indicates a linear relationship, and the observed deviation from linearity is noted by the top curve. Dale et al. defined a "damage enhancement factor" as the ratio of observed damage factor ratio (upper line) to that expected based on the linearity with NIEL (lower line). In this work, the PKA spectrum produced in Si by the various incoming particles was calculated. Note that the PKA spectrum varies significantly over the range of proton energies of interest in space. It may come as a surprise that the PKA spectrum of a 60 MeV electron is more like that of a 10 MeV proton, than a 10 MeV proton is like a 60 MeV proton. As seen in figure 8, the damage enhancement factor is found to correlate with the fraction of the total NIEL due to PKAs with energies less than 1 keV. It is notable that the result held for the wide range of PKA spectra produced by 4.1 MeV electrons, all the way to 1 MeV-equivalent neutrons that produce very high energy recoils. The observed deviations from linearity

would be expected if there were less recombination of initial vacancy-interstitial pairs that are formed by lower energy PKAs (which produce well-separated Frenkel pairs). This result is consistent with the previously described Monte Carlo calculation of collision cascades showing that the more dense subcascades do not begin to form until PKAs have energies over about 2 keV. Later measurements of the CTE degradation in Si CCDs (from 2 manufacturers) over a wide range of proton energies also reveal enhanced damage at lower proton energies [Dale93]. However, we note that such deviations were not apparent in a study by Luera et al. [Leur87].

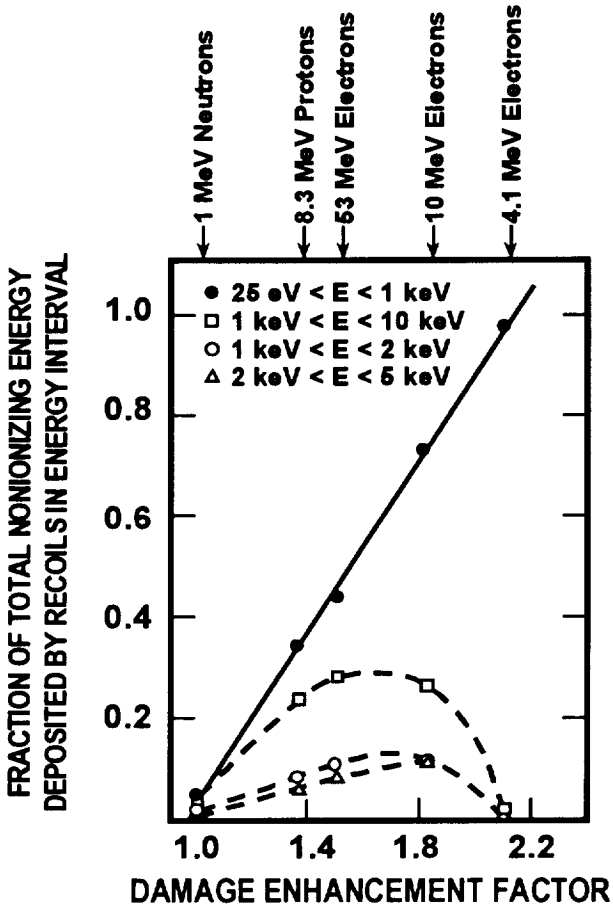

Figure 8 The correlation between percent NIEL in Si due to recoils in the various energy ranges and the magnitude of the deviation from the ideal linear dependence is shown. The particles associated with a given deviation are labeled at the top of the figure. After [Dale88].

Evidence that lower energy protons are more effective at producing displacement damage in GaAs as compared to higher energy protons (than the NIEL correlation would indicate) has been reported by Luera et al. [Luer87, Grif91] and Barry et al. [Barr95]. These studies were based on measurements of carrier removal in Van der Pauw samples and minority carrier lifetime degradation in LEDs. Once again, the results were explained by variations in the recombination efficiency of the Frenkel pairs with PKA energy. In 1995, Barry et al. extended measurement of the minority carrier lifetime

damage factors in GaAs LEDs to proton energies as high as ~500 MeV [Barr95]. Figure 9 compares these results with the NIEL calculation by Burke [Burk87]. Other results in the literature also indicate departures of damage factors from the NIEL energy dependence [Zhao97, Summ88]. Although the 1993 paper by Summers et al. claims to have demonstrated a general linear correlation between device "proton damage coefficients" and NIEL for Si, GaAs and InP, using "solar cells as examples," it is important to note that the data presented do not cover the relevant range of proton energies for most satellite applications which are more heavily shielded. For example, both the GaAs data (from [Ansp92]) and the InP data (from [Yama84]) are for protons below 20 MeV, and are indeed most relevant to lightly shielded solar cell applications. It is interesting to note that a recent paper based on the same solar cell data set [Ansp92], shows damage coefficients falling below the calculated GaAs NIEL at higher proton energies [Walt99], consistent with figure 9. (The authors did not discuss this trend which was not relevant to their recent solar cell study.) Clearly, further efforts are required to better understand the nature of these deviations.

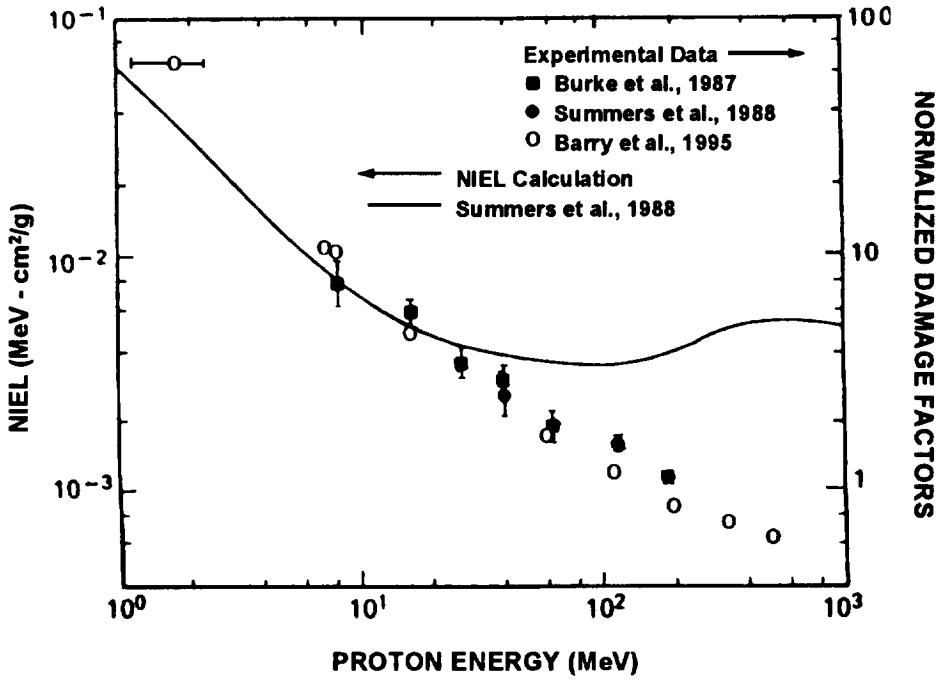

Figure 9 Experimental damage factor from several studies are normalized to the GaAs NIEL calculation at 10 MeV. A significant deviation between the observed damage factors and NIEL is apparent for proton energies above about 40 MeV. Adapted from [Barr95].

During semiconductor research efforts in 1950s, it was noticed that NIEL calculations (which compute that portion of the total energy deposited via non-ionizing interactions) significantly over-estimated defect production. Analytic expressions were developed with *energy dependent* damage efficiency coefficients that represented the likelihood that the initial Frenkel pairs would survive recombination, and experimental efforts confirmed this behavior in metals [Aver83, Hein83]. If the space radiation effects

community plans to use *calculated* displacement damage functions to describe the energy dependence of device response for more than rough approximations, it needs to move beyond NIEL calculations and investigate the time evolution of the initial damage to a variety of electrically active defects. It is not clear to what degree the physical processes need to be modeled in order to derive a sufficiently accurate damage function for use by the radiation effects community.

In the meantime, the satellite designer must typically make on-orbit device performance assessments based on laboratory radiation measurements at one (or at most a few) proton energies, and therefore must make an assumption concerning the energy dependence the measurements will follow. There are several possible approaches including use of: (1) a calculated NIEL curve, (2) an experimental displacement damage curve (if available), or (3) a piecewise "manufactured" worst case displacement damage function. All of these approaches have significant uncertainty associated with them that must be reflected in the design margin applied to a given application.

2.3.3 Calculation of Displacement Damage Equivalent Fluences

It is very useful for the radiation design engineer to become comfortable with the calculation of damage equivalent fluences (and displacement damage dose). Data in the literature are collected using a variety of incident proton energies, and one needs to be able to convert to an equivalent fluence at a particular energy of interest. (The respective fluences are "equivalent" in the sense that they will produce the same amount of displacement damage in the device.) Likewise, it may be necessary to convert the proton spectrum for a particular mission to an equivalent fluence at a specific proton energy.

To the extent that the proton energy dependence of the device degradation correlates with NIEL (or a relevant measured damage function), radiation testing can (in principle) be performed at only one proton energy. In practice, we have seen that there can be significant uncertainty in the energy dependence of the device radiation response. Nevertheless, program constraints often restrict proton testing to a single energy, and it is important to choose the test energy very carefully. We will see in section 2.4 that we can use our displacement damage analysis tools to select appropriate test energies, and that the choices will depend on the degree of device shielding in a particular application.

Many of the space applications employing photonic devices (e.g., CCDs, etc.) are heavily shielded, and the peak in the transported proton spectra is shifted to higher energies, typically between 40-100 MeV. (Refer to part IVA, section 2 for a description of proton environments and shielding.) For this reason, and because package penetration and energy deposition uniformity issues are simplified when very penetrating protons are used, higher energy protons are frequently employed for radiation tests. In this approach any error introduced by a lack of correlation between the measured property and the displacement damage function is minimized. The optimal choice for a single test energy is the one that best represents the *damage-weighted* proton spectrum calculated using a displacement damage function. As illustrated in the next section, one can calculate the

differential or integral displacement damage energy deposition as a function of proton energy and use these results to aid in the selection of proton test energies [Dale91].

Once one or more proton test energies have been chosen for a particular space mission, the relevant MeV-equivalent fluences can be calculated using the calculated NIEL (or an experimental damage function) and the differential proton fluence spectrum, $d\Phi(E)/dE$, for the time period of interest. Note that a given mission may be represented by a time-weighted sum of more than one differential spectrum depending on the details of orbital precession, solar cycles, etc. The MeV-equivalent proton fluence at a given test energy, E_{test} is given by:

$$\Phi(E_{test}) = \frac{\int_{E1}^{E2} \frac{d\Phi(E)}{dE} NIEL(E)dE}{NIEL(E_{test})} \tag{5}$$

where the numerator is just the total displacement damage dose in units of MeV/g when NIEL(E) is expressed in units of $MeVcm^2/g$. The integration limits, E1 and E2, generally correspond to the lowest and highest proton energies provided in the differential spectrum, typically from about 0.01 MeV to about 500 MeV. Note that the range of integration may be reasonably adjusted depending on the degree of shielding present [Dale91, Mess97]. As an example, a 60 MeV-equivalent fluence is simply the fluence of 60 MeV protons that produces the same amount of displacement damage dose as the time-integrated transported proton spectrum representing the mission environment.

Equation 5 can also be used to calculate the mission equivalent fluence at a proton energy for which there is relevant device data in the literature. In this way, one can assess the suitability of a candidate device for a particular mission, or (as often is the case) to provide an initial assessment of a device already chosen. The NIEL correlation may also be used to estimate the relative damage of protons and neutrons, which is useful since there is a large body of literature concerning neutron induced displacement damage.

In the case of solar cell applications, minimal shielding is utilized. As a result such devices are subject to displacement damage dose from both electrons and relatively low energy (and more damaging) protons. In the solar photovoltaic community, it is customary to compare the degradation of various technologies to their response to 1 MeV electron irradiation. The on-orbit proton environment is expressed as a 10 MeV proton equivalent fluence, and then converted to a 1 MeV electron equivalent fluence [Tada82].

2.3.4 Concept of "Displacement Damage Dose"

The concept of non-ionizing energy deposition (e.g., NIEL) plays the same role in displacement damage effects as the ionizing energy deposition (or linear energy transfer (LET)) plays in ionization induced effects [Dale89a]. The units are the same, namely MeV/g. Although displacement damage dose has not yet been treated formally as a unit of dose, the radiation effects engineer may, for practical purposes, define a unit of displacement damage dose as 100 ergs of non-ionizing energy deposited per gram of

material. This approach was introduced in 1991 to quantify displacement damage dose effects and simplify on-orbit predictions for the charge transfer efficiency (CTE) in CCDs [Dale91, Dale92b]. The advantage of this method is that a single unit provides a simple way to compare the effective amount of displacement damage resulting from any specified space environment or proton fluence at a given test energy. In fact, it was initially introduced as a "non-ionizing rad", or NIRad(Si), as part of an introductory tutorial for the non-radiation effects personnel in the astronomy community. They were the first to attempt using extremely high quality scientific CCDs in demanding space applications. Since the concept of an ionizing rad(material) is generally familiar to design engineers, it is a useful way to implement a displacement damage analysis tool.

Within the radiation effects community, equivalent displacement effects have long been expressed in terms of 1 MeV neutron equivalence [see Mess86, Gove84]. In the last decade, several groups have advocated the usage of various proton energies as the MeV-equivalent comparison of choice. However, the best energy choice is made by consideration of the transported damage-weighted proton spectrum that is very dependent on the shielding material and thickness. For example, a 10 MeV-equivalent proton "standard" might be used for a thinly shielded solar cell project, whereas a 60 MeV-equivalent proton "standard" might be chosen for a heavily shielded CCD study. As discussed below, displacement damage can easily be compared in terms of "equivalent proton fluences" at one of these specified energies. *Whether one chooses to perform a displacement damage analysis in terms of displacement damage dose or a MeV-equivalent fluence, it is very important to identify the damage function employed since the final result can depend critically on this choice.*

2.4 On-Orbit Performance Predictions

In this section, we will first describe a method for performing space predictions based on the concept of displacement damage dose described above. In practice, it is useful to consider two important cases. In the first, the device parameter of interest (e.g., CCD CTE or dark current) varies linearly with proton fluence (i.e., can be characterized by a damage factor). In the second, the device property of interest (e.g., current transfer ratio of an optocoupler or the maximum power of a solar cell) behaves nonlinearly with proton fluence. In both cases, the energy dependence of the property in question may be assumed to follow the calculated NIEL, and the concept of displacement damage dose in units of MeV/g is employed. (Note that, as discussed above, the NIEL may be replaced by a damage function constructed to provide a worst case performance analysis.) This predictive tool was first used to predict on-orbit CTE in Si CCDs [Dale91, Dale93], but the interested reader can refer to the literature to learn more about this approach as applied to other applications (e.g., InGaAs detector dark current and responsivity predictions [Mars94] and solar cell characterization in space [Sum94, Mess97, Walt99]).

We will first illustrate the basic method for performing space predictions for the case where a damage factor can be defined, by calculating the yearly on-orbit CTE degradation for CCDs. Although the present section focuses on the predictive tool itself,

we note that some of the issues raised will be explored in more depth in section 3.2.2, which concentrates on displacement damage in CCDs.

The first step is to define the relevant damage factor, and determine the most appropriate damage function to describe the energy dependence of this damage factor. In the present case, we consider the CTE damage factor, K(E), defined as the change in CTE per unit proton fluence, Φ(E) as shown:

$$\Delta CTE(E) = K(E) \cdot \Phi(E). \tag{6}$$

The change in CTE is dominated by bulk displacement damage and therefore linear with proton fluence. The experimental CTE damage factors are shown in figure 10, together with the NIEL calculated in Si. The data from each CCD type exhibit a similar energy dependence, and each data set has been independently scaled to NIEL using a constant, C, which has units of CTE change per unit of non-ionizing energy deposited. Hence, we have

$$K(E) = C \cdot NIEL(E). \tag{7}$$

Recall that a scale factor is necessary because it is not presently possible to make a first principles calculation of the final stable proton induced defect inventory (defect types and quantities), and its effectiveness at causing CTE changes. (The exact value of this constant also depends on a particular imager design and the readout conditions as will be discussed in section 3.2.2.)

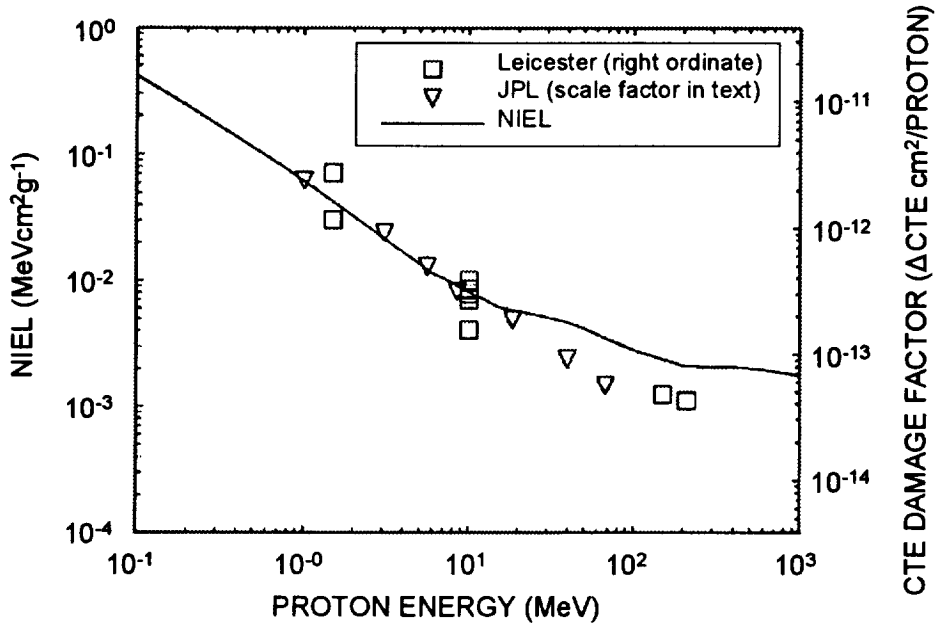

Figure 10 The NIEL is compared with experimental CTE damage factors. The data was normalized to NIEL at 10 MeV, and the scale factor values are 3.9×10^{-11} and 1.2×10^{-11} ΔCTEg(Si)/MeV for the Leicester (EEV) and JPL (Ford) CCDs, respectively. At higher energies,

the data fall below the NIEL curve. The deviations from NIEL are consistent with those observed in figure 7 for a different set of devices. After [Dale93].

Figure 10 also shows that the measured CTE damage factor falls below the NIEL calculation at higher energies, for reasons still not well understood (see section 3.2.2). In this example, we perform the on-orbit prediction using the theoretical NIEL calculation as the displacement damage function, in order to provide a conservative engineering estimate of performance. It turns out that the CTE degradation is over-estimated by a factor of two by using the NIEL dependence instead of the energy dependence of the measured damage factors.

The final information needed for the on-orbit prediction is the differential proton spectral information, $d\Phi(E)/dE$, for the orbit and shield thickness in question. This is used to calculate the amount of displacement damage at each proton energy for the time period considered. The total damage follows from integrating the damage over all energies reaching the CCD as expressed below:

$$\Delta CTE(E) = \int_{E1}^{E2} K(E)\frac{d\Phi(E)}{dE}dE = C\int_{E1}^{E2} NIEL(E)\frac{d\Phi(E)}{dE}dE\,. \qquad (8)$$

Note that the integral is simply the displacement damage dose in units of MeV/g when NIEL(E) is expressed in units of $MeVcm^2/g$. The integration limits, E1 and E2, are defined and discussed with equation 5.

Despite various mitigation approaches, for devices such as CCDs that are extremely sensitive to displacement damage, it is often necessary to resort to the use of thick shields to minimize the radiation damage at the CCD location. As we will explore in section 3.1.2, displacement damage effects from secondary particles (mostly neutrons) produced in thick shielding can be significant, especially for high atomic number shields such as Ta. To calculate the effects of more than one particle type (such as secondary neutrons produced in shielding), the contribution for each particle is computed independently, as discussed earlier. The NIEL for neutrons in Si is described in [Dale91].

Figure 11 shows the results of equation 8 for the EEV imager in the 705 km, 97.4° polar orbit for four Al shield thicknesses, including the effects of secondary particle damage. The integral displacement damage dose and ΔCTE due to protons above a given energy are obtained by evaluating the integral from E to the highest proton energy. The intercepts show the effects of particles of all energies in terms of non-ionizing energy deposited per gram Si per year, or as the ΔCTE per year. We see that the relative gains from adding shield mass diminish as the shield gets thicker. Also, except for lightly shielded imagers, most of the damage results from protons over 10 MeV. These calculations are useful for determining the most relevant proton test energies for a particular shielding configuration. It can come as a surprise to discover that, in a heavily shielded application, half (or more) of the displacement damage dose is contributed by incident protons with energies in excess of 100 MeV. This is true despite the fact that lower energy protons produce more displacement damage, because the transported proton spectra are becoming much harder with increasing shield thickness. The spectral

hardness occurs because the lower energy incident particles have a higher LET and are therefore preferentially stopped in the shielding.

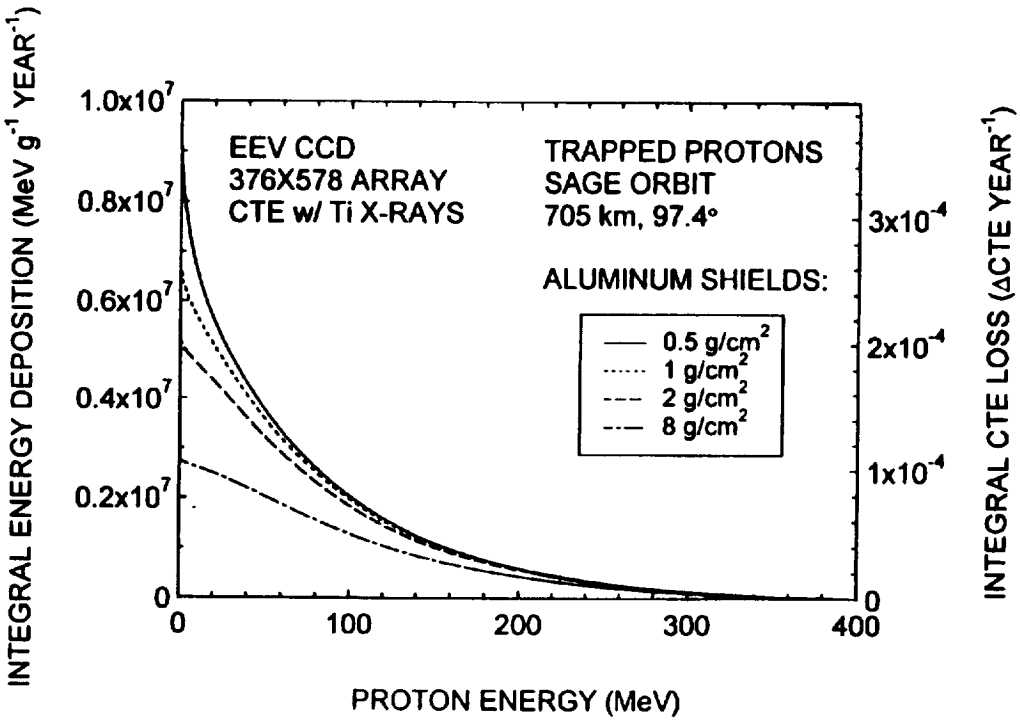

Figure 11 The integral damage spectrum (integrated from the energy in question to the highest proton energy) is shown versus proton energy. The intercepts at zero energy give the yearly total damage for the entire proton spectrum. The values in order of increasing shield thickness are $9.2\text{x}10^6$, $6.7\text{x}10^6$, $5.3\text{x}10^6$, and $2.93\text{x}10^6$ MeV g(Si)$^{-1}$ year^{-1}. The corresponding CTE losses per year given from the right ordinate are $3.6\text{x}10^{-4}$, $2.6\text{x}10^{-4}$, $2.0\text{x}10^{-4}$, and $1.1\text{x}10^{-4}$, respectively. After [Dale93].

In some cases, the device parameter of interest does not degrade linearly with proton fluence (or displacement damage dose). This behavior has been observed for the degradation of optocouplers [John96, Reed98] and solar cells [e.g., Ansp92, Yama96, Mess97, Walt99], and is discussed further in sections 3.3.5 and 3.3.6. In this case, we measure the device response as a function of displacement damage dose (or MeV-equivalent fluence at an agreed upon energy) to assess device performance in relation to the mission requirements. (Care should be exercised when the mission requirement falls in a regime where the device response is changing rapidly with increasing damage dose.) Note that the underlying assumption in this case is still that the device degradation correlates with the NIEL as a function of proton energy. To the extent that this is true, the curves measuring the device degradation as a function of fluence for various proton energies will fall on a common curve if they are plotted versus proton dose calculated using NIEL.

In summary, the NIEL-based methodology provides the satellite designer with an invaluable tool for estimating on-orbit degradation due to displacement damage and making use of the displacement damage literature, providing they are used with caution. This is particularly true since the radiation engineer must typically make assessments based on device radiation measurements at one (or at most a few) proton energies, which requires the use of an energy dependent damage function. However, in many cases, the biggest challenge to the satellite designer is to identify a laboratory radiation test that provides an accurate indication of the on-orbit performance to be expected for a given device or subsystem. In the case studies to follow, we will find that the radiation response of a device is very application specific, and that it is sometimes nontrivial to design a relevant laboratory radiation test.

3.0 PROTON DISPLACEMENT DAMAGE CASE STUDIES

3.1 Introduction

The following case studies provide examples of the analysis tools presented in Section 2.0, and illustrate the range of issues that can arise in the attempt to assess on-orbit performance based on laboratory radiation test programs and displacement damage analysis. The device types represented are those of current interest for which displacement damage issues can be significant. Of course, the complete assessment of a device or technology for use in a space environment demands that all radiation induced degradation be considered including total ionizing dose (TID) and single-event effect (SEE) issues from protons and heavy ions, as appropriate. In some cases, devices that are sensitive to displacement damage also have a noticeable TID response. In general, a good engineering radiation assessment of on-orbit displacement damage effects can be made based on the results of laboratory tests at a proton accelerator. As discussed in section 2.3.3 and 2.4, proton test energies should be wisely chosen based on the shielded proton environment at the device of interest. In this case, the effects of both displacement damage and TID are simulated reasonably well.

3.2 Laboratory Radiation Test Issues

For any application where displacement damage is expected to produce significant degradation, it is important to perform a proton radiation test in addition to the routine Co-60 TID evaluation. In some cases (e.g., CCDs), the combination of limited device availability and time-consuming measurement procedures results in the use of proton irradiations to evaluate both the TID and displacement damage response of a device. Recall from the discussion in section IVA, that "a rad is a rad" is a reasonably good assumption for proton energies above about 40 MeV, and it is therefore straightforward to calculate the proton induced TID.

If concurrent TID effects are significant, then it is important to design the proton test with appropriate controls on the bias, measurement timing, etc. as described in

standard TID test methods such as MIL-STD-883, Method 1019. In such cases, there is always the possibility that the failure mechanism (TID versus displacement damage induced) depends on the ionizing dose rate employed in the test. Obviously, this is a concern since typical space dose rates are many orders of magnitude lower than those employed in laboratory proton measurements. Although it is possible to perform lengthy low dose rate testing at a Co-60 source, such testing is not feasible at a proton facility.

In some cases, the relative importance of TID versus displacement damage dose may not be well characterized for a particular device. For example, the susceptibility of linear bipolar ICs to displacement damage and TID varies over a wide range because of significant variations in device design and processing techniques [Gaut83, John87, Rax97, Rax98]. A recent study of modern bipolar technology provides general guidelines to help identify cases where displacement damage is most important [Rax98], but sometimes this is best determined by comparing test results for both proton and Co-60 exposures. Comparisons are made either by plotting the device degradation as a function of equivalent TID or displacement damage dose. Note that it is generally not possible to separate out the relative importance of TID versus displacement damage dose by comparing exposures at different proton energies. This is because both effects exhibit a qualitatively similar energy dependence as illustrated in figure 5.

As will be discussed in section 3.3.5, optocouplers may also be subject to both TID and displacement damage effects [John96, Reed98]. DC-DC converter modules also may fail from either displacement damage or TID degradation, depending on whether the unit uses an optocoupler for isolation. Since CCDs are MOS devices, they are also subject to TID degradation. Although the performance of many CCD devices is limited by displacement damage, those from some manufacturers fail by TID induced threshold shifts in output circuitry. In many cases, it is useful to monitor the device properties after proton irradiation to look for substantial recovery which can be the signature of a device that has failed to function as a result of TID exposure at laboratory dose rates. (This practice can prevent the unnecessary disqualification for a device for space use. Note that this practice is consistent with the Method 1019 standard [Sext92] used for Co-60 tests. This procedure permits a room temperature anneal as a surrogate for a low dose rate test, as long as the device does not fail functionally.) Once again, the comparison of proton and Co-60 test results can help to sort out failure mechanisms.

In the case of multi-component modules, one must always consider the possibility of both TID and displacement effects. For example, modules containing photonic devices expected to degrade via displacement damage mechanisms may also contain passive elements (e.g., lenses) that degrade from TID effects. Recently, the response of an InGaAsP laser module to protons was found to be dominated by darkening in a graded index (GRIN) lens, even though the laser itself was quite hard to displacement damage [Mars92]. (This behavior was confirmed through the use of additional Co-60 testing.) Given the wide range of hardness in lens materials, it can be useful to perform a cheaper Co-60 screening test of such modules *before* proton testing.

Proton test energies should be selected based on the particular application, as described earlier, but it is always important to ensure that the incident proton has sufficient range to penetrate both the device packaging and the sensitive volume of the device itself. The analysis is greatly facilitated (and more accurate) if the non-ionizing energy loss rate through the active volume of the device is constant, and if the incident proton beam is reasonably monoenergetic.

In some cases, the active volume of a device may be very thin, and also close to the surface of the device. If such a device is irradiated with protons normally incident to the surface, the forward directed energetic recoils may deposit their energy below the active device region. As shown in figure 12, it can take several microns to reach "recoil equilibrium" inside a device [Dale94]. Since recoil equilibrium applies to devices in a shielded spacecraft subject to irradiation from all sides, we also should approximate this condition in laboratory radiation tests. If it is questionable whether a device will be in recoil equilibrium for the case of protons incident from the front, the unit may simply be irradiated from the back to achieve equilibrium. This effect may have been at least partly responsible for deviations of Si CCD damage factors from NIEL observed at higher proton energies in figure 10 [Dale94]. Lack of recoil equilibrium was cited in [Summ88] as a possible explanation for the deviations of Si JFET damage factors from NIEL apparent in figure 9. However, Barry et al. [Barr95] eliminated recoil equilibrium as an explanation for the deviation of their LED damage factors from NIEL by also irradiating devices from the backsides with identical results. Although this issue has not been well studied, it is nonetheless straightforward to perform proton irradiations so that recoil equilibrium is satisfied.

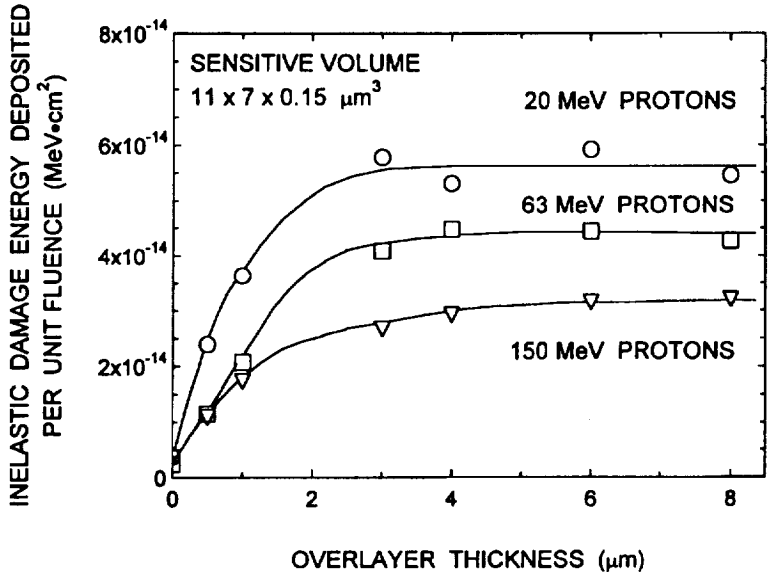

Figure 12 The approach to displacement damage equilibrium is shown for several proton energies. It is also shown in [Dale94], that the overlayer thickness required to achieve equilibrium increases as the thickness of the sensitive volume decreases. After [Dale94].

One frequently asked question is whether or not a device (*whose radiation response is dominated by displacement damage up to the fluence in question*) may be passively exposed to protons, and then characterized in depth once transported back to the laboratory. In many cases (but not all [e.g., Sun99]), relatively little long term annealing of displacement damage occurs, so that it can be reasonable to irradiate a device, and then return it to the laboratory for testing at a later date. It is generally good practice to ground the device leads during the proton exposure to prevent the possibility of electrical discharges. In most cases, displacement damage induced degradation at the device level is found to be independent of the bias during irradiation. An important exception is photonic devices (e.g., lasers, LEDs and solar cells) fabricated from compound semiconductors that may exhibit bias-dependent degradation and annealing (see section 3.3.4).

Finally, it is essential for the radiation effects personnel to interact closely with the appropriate applications engineer on the design of laboratory radiation tests. In general, the radiation response of a device or subsystem is very application dependent. For example, the proton induced degradation observed in optocouplers is very dependent on the operating conditions (e.g., the LED drive current, the phototransistor collector-emitter voltage, and the load). A second example is the proton induced degradation in the CTE of a CCD which depends strongly on the temperature, signal size and pattern, readout rate, and other factors [e.g., Hopk96, and references therein]. Hence it is critical to choose a measurement technique that reflects as closely as possible the on-orbit operating conditions. In some cases (including the CTE measurement), one of the biggest challenges to the satellite designer is to identify a laboratory radiation test that provides an accurate indication of the on-orbit performance expected for a device or subsystem.

3.3 Case Studies

3.3.1 Bipolar Transistors

As discussed earlier, discrete bipolar transistors have served as important test vehicles to study displacement damage effects, but this should not be construed to imply that such devices would be primarily degraded by displacement damage effects on-orbit. Quite the opposite is true. (In order to isolate displacement damage induced effects, the devices in these studies are pre-irradiated to multi-megarad levels with Co-60 to saturate the ionization damage prior to the proton, neutron and heavy ion exposures [Summ86]. Also, such studies may choose not to operate devices with low current bias so as to minimize surface currents.) Much of the early displacement damage work on bipolar transistors focussed on neutron induced degradation and provides the basis for the current understanding the proton effects [e.g., Mess86]. Neutron induced degradation of the DC gain, drive current and V_{CE} were explored and mitigation approaches derived. Although radiation effects research has resulted in hardened discrete bipolar devices, there continue to be displacement damage concerns, particularly for analog bipolar IC applications.

The susceptibility of linear bipolar ICs varies over a wide range because of significant variations in processing, device design and specific performance requirements [Gaut83, Gove84, Mess86, Raym87, John87, Rax97, Rax98]. In general, it has been found that devices that contain substrate or lateral pnp transistors are most sensitive to displacement damage as a result of degradation of the minority carrier lifetime in the wide base regions (i.e., low f_T, or gain-bandwidth product). Circuit level design also plays a large role. For example, the use of a lateral pnp transistor as a primary input transistor operating at low current levels would be expected to increase the device vulnerability to degradation from displacement damage. A recent study by Rax et al. provides another example of a design practice that results in proton sensitivity [Rax98]. Figure 13 shows test results for an operational amplifier that fails its specification limit at an equivalent ionization level that is only 60% of that observed during gamma irradiation [Rax98]. The authors found that the output stage of the circuit is asymmetrical; it sources up to 10 mA, but is only guaranteed to sink 1 mA. It relies on the gain of a single substrate pnp transistor to sink current from an external load, making it quite susceptible to displacement damage as a direct result of circuit design.

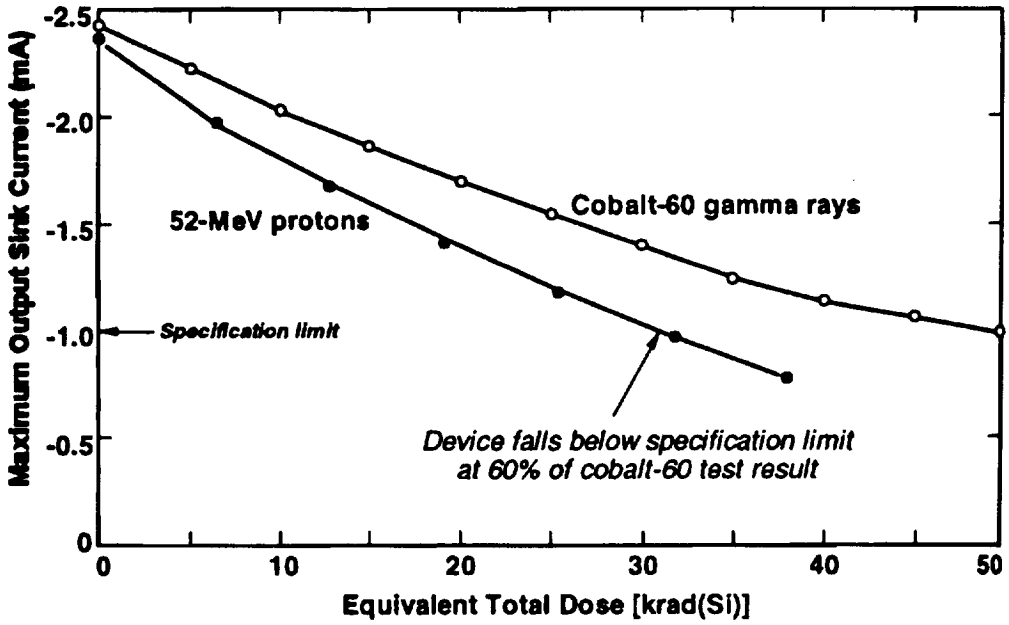

Figure 13 The degradation in the output sink current of an OP221 operational amplifier is significantly more pronounced for proton (as compared to gamma) irradiation. The sensitivity to displacement damage is a direct result of a specific design technique. [After Rax98].

As expected, a precision, high performance linear application using a device with demanding electrical specifications will be significantly more sensitive to displacement damage induced degradation. For example, an application may require a very low input offset voltage, and/or input offset and bias current, or low noise. Recently Rax et al. found significant differences between proton and gamma ray results, which showed that displacement damage could be important, even in precision reference circuits that rely primarily on high f_T npn transistors [Rax97]. As described in the last section, laboratory

test results must be carefully interpreted since the actual failure mode and sensitivity to displacements can depend on the specific environment (e.g., relative amounts of TID and displacement damage dose), and the device circuit and operating conditions.

In contrast, heterojunction bipolar transistor (HBT) technology is known to be robust in a proton environment. Ohyama et al. have investigated the proton induced degradation of SiGe HBTs as a function of Ge content [Ohy96]. In addition, Roldan et al. [Rold98] have recently investigated the effects of 46 MeV proton irradiated induced trap generation and its impact on the electrical characteristics on SiGe HBTs from a state-of-the-art IBM BICMOS commercial technology. After 10^{14} cm^{-2} protons (18.4 Mrad(Si) equivalent TID), the peak current gain (at 10 μA) was reduced by <8% and the maximum oscillation frequency and cutoff frequency showed only minor degradation. As we saw in the previous discussion of Si linear bipolar technology, the lateral pnp transistor exhibits an enhanced sensitivity to both TID and displacement damage. Recently Niu et al. investigated proton effects in gate-assisted lateral pnp (GLPNP) transistors from the advanced SiGe HBT BICMOS technology [Niu98]. They isolated the effects of proton induced bulk traps from those of surface traps and oxide charges in the GLPNP transistors that are widely used in BICMOS circuits [Niu98]. Negligible current gain degradation was observed for 46 MeV proton fluences of 10^{12} cm^{-2}, and the devices were still functional at 10^{13} cm^{-2}. The authors attribute the improved radiation hardness of this technology (as compared to conventional lateral pnp's) to the much thinner oxide and gate-assisted operation that minimizes the TID response. Clearly this technology is quite insensitive to both TID and displacement damage effects.

3.3.2 Charge Transfer Devices

Silicon optoelectronic sensing arrays (visible, UV and x-ray) have been developed for a wide variety of scientific, commercial and military uses in space. They contain a matrix of up to several million photosensitive elements (or pixels) which generally operate by converting the photo-generated charge to a voltage that is multiplexed to a small number of output amplifiers. Present charge coupled devices (CCDs) are available with picoampere dark currents and charge transfer efficiencies (CTE) in excess of 0.999999 per pixel. During the development of these sensors, their susceptibility to ionizing radiation effects has been characterized and hardening solutions have been successfully implemented in many cases. The most commonly used CCD for visible and UV detection is the buried channel device which has a shallow n-type layer implanted below the surface to keep the stored signal charge away from the traps associated with the Si/SiO_2 interface. Such CCDs may be hardened to TID effects either by the use of radiation hardened oxides [Carb93], or by biasing the device so that the silicon surface is inverted so that the interface traps are filled and dark current generation is suppressed [Saks80]. This can be achieved with an extra implantation to form a multiphase pinned device [Jane95], or by shuffling the charge back and forth between gates within a pixel faster than the surface states can respond (so-called dither clocking) [Burk91, Hopk92].

Bulk displacement damage effects often dominate the radiation response in state-of-the-art scientific imagers when operated in natural particle environments

[e.g., Jane91, Holl91b]. The flatband shifts and dark current increases that occur for ionizing dose levels below 10-20 krads(Si) are often not serious, and can be overcome with minor changes in voltages and operating temperature. In contrast, significant CTE losses are observed for proton exposures of less than 1 krad(Si). Nevertheless, the degree of CTE loss that is tolerable is very application-dependent, and it is still possible for a device to ultimately fail as a result of either TID or displacement damage effects at higher exposure levels. It is important to verify that flatband shifts will not take a device out of inversion prior to the expected mission dose, and also to ensure that the readout amplifier circuitry is robust. A detailed description of proton effects in CCDs may be found in a recent review article [Hopk96] and references therein. Displacement damage degrades CCD performance by decreasing the CTE, increasing the average dark current, by introducing individual pixels with very high dark currents (or "spikes"), and by increasing the noise of the output amplifier. An overview of each of these effects follows.

One of the most important performance parameters for a CCD is the CTE, which is the fraction of signal charge transferred from pixel to pixel during read out. Arrays with 1024 x 1024 pixels (and larger) are routinely used today, and require very low trap densities in order to operate correctly. For example, to reduce signal loss to less than 10% for 1000 pixel-to-pixel transfers, a CTE of at least 0.9999/pixel is necessary. For a typical device with 50 μm^3 pixel volumes, this corresponds to less than one radiation induced defect every ten pixels, which can easily be exceeded during a typical space mission [Hopk96]. If a signal charge is trapped by a proton induced defect, and remains trapped for more than one clock cycle, it will be lost from the signal charge packet. The trapped charge is eventually re-emitted into trailing pixels, and produces a smeared image. It is the interplay between the temperature dependent carrier emission and capture dynamics of the radiation induced traps and the device readout scheme and clocking rates that determine the CTE behavior of an irradiated CCD [Mohs74].

To understand this interplay, we consider the readout procedure for a 2-dimensional CCD array. Signal charge packets are stored in the depletion regions formed underneath a biased gate during the integration period. Since the gate voltage determines the potential well capacity underneath, the signal charge can be moved down the rows in the buried channel by the appropriate sequencing of the gate voltages as indicated in figure 14a. The charge is confined laterally to a single row by an implanted channel stop. After each "parallel" transfer of the charge from one pixel to the next, the charge packet is clocked out of the serial register as depicted in figure 14b, and the whole process repeated until the imager readout is complete. Unfortunately, the time to read out the serial register is long enough for signal charge to be trapped. The signal charge can subsequently be re-emitted into a trailing pixel thereby degrading the CTE. Since the carrier emission times depend exponentially on temperature, the CTE response of a 2-dimensional CCD array is a strongly temperature dependent. In contrast to the typical area array, the linear CCD with clocking speeds at 1 MHz or more is relatively immune to proton induced CTE degradation. This is because the capture times for key radiation induced defect levels, such as the E-center, are too long relative to the charge transfer rate for the traps to efficiently trap signal charge. Further details of radiation induced CTE

degradation are beyond the scope of this course, but are described in detail in many papers, including [Mohs74, Bang91, Dale93, Jane95, Hopk96].

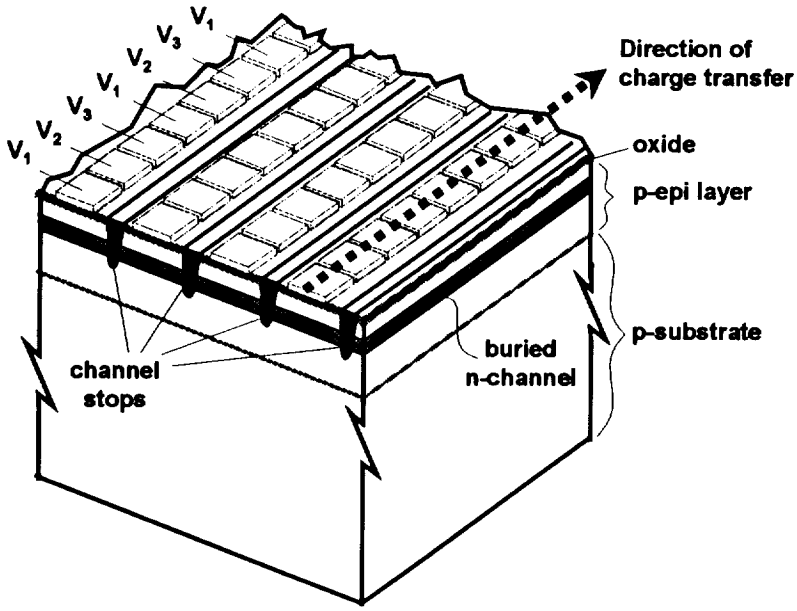

Figure 14a Illustration of parallel charge transfer down a row of MOS capacitors. A 3 phase CCD is pictured, in which each pixel is composed of 3 electrodes for charge transfer. The signal charge travels in the buried channel and is restricted to a single row by implanted channel stops.

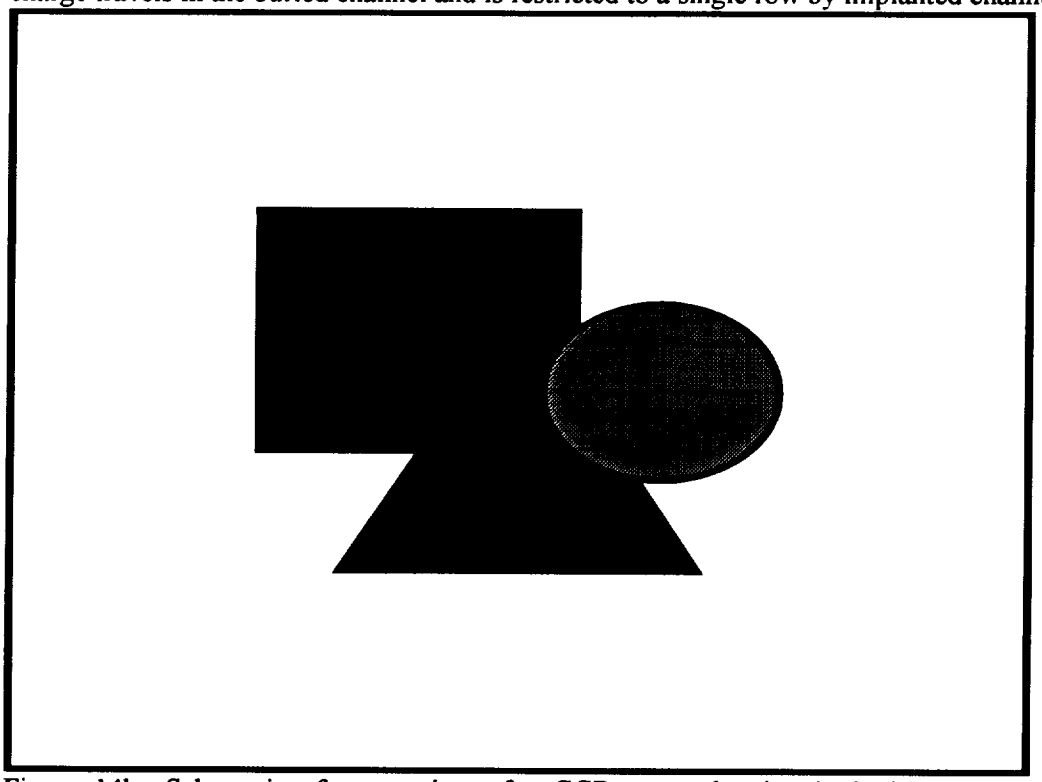

Figure 14b Schematic of a top view of a CCD array showing both the parallel and serial readouts. CCD evaluations include measurements of both the parallel and serial CTE.

Unfortunately, efforts to harden CCDs to displacement damage have not been nearly as successful as TID hardening. However, displacement damage effects can be ameliorated using several techniques. CTE loss can be somewhat reduced by substantial cooling (often to about –80 °C), to mitigate the trapping effects of the E-center (and also minimize dark current). As illustrated in figure 15, background charge can dramatically impact the CTE loss by filling the traps so that they do not interact with the signal charge packet. The magnitude of the improvement depends on the signal size, and usually (though not always [Robb92]) comes at the price of additional noise. Another CTE hardening technique employs an additional phosphorus implant to confine the signal charge to a smaller volume (referred to as a notch or minichannel) so that fewer traps are encountered as the signal charge is read out. Notches may be useful for low signal level applications and some CCD operating conditions, but the efficacy of a notch may vary considerably between manufacturers (or even lots from a single source). Further information concerning mitigation techniques may be found in [Hopk96] and references therein.

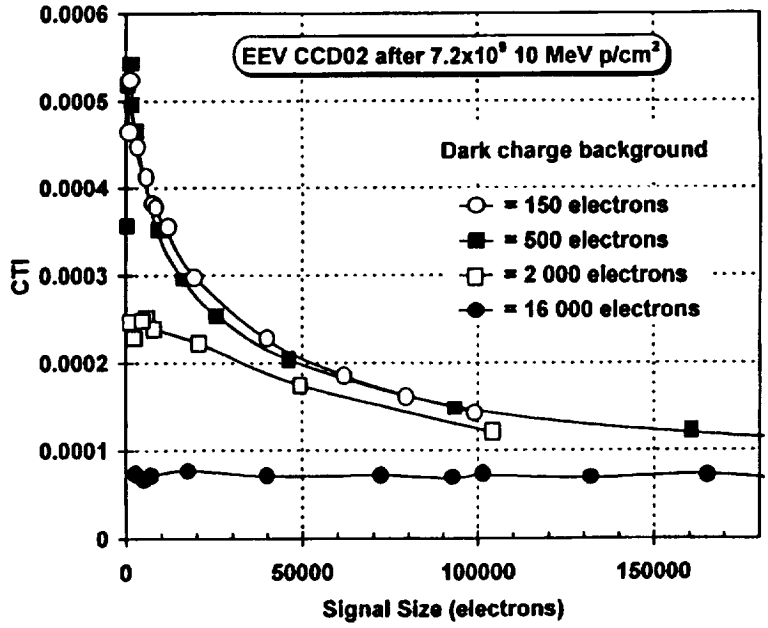

Figure 15 The charge transfer inefficiency (CTI = 1-CTE) for a CCD exposed to a proton fluence of 7.2×10^9 cm^{-2}, corresponding to TID of 4 krad(Si). Both the CTI and the efficacy of a dark charge background in CTI reduction are a function of signal size. After [Hopk94b].

For most satellite programs these mitigation techniques are not sufficient, and one must resort to shielding. Recall from part A of this segment that protons are not easily shielded against. In fact, quite thick (a cm or more) of high atomic weight shielding (e.g., Ta or W alloys) may be used to minimize displacement damage to the CCD. Recall that in section 2.4, we used the Si NIEL correlation together with measured CTE damage factors to predict the on-orbit performance of a CCD. The results were displayed in figure 11 for several shield thicknesses, and confirmed the need for substantial shielding to maintain reasonable CTE performance in space. However, for heavily shielded

devices, the displacement damage caused by secondary particles produced in the shielding itself is significant, and in some cases dominant [Dale93]. (Incoming protons may interact with the atoms in the shield material causing nuclear reactions that produce secondary particles such as neutrons and protons.)

The NIEL prediction methodology presented in section 2.4 is readily extended to include the displacement damage effects of secondary particles on CTE degradation. Figure 16 shows the relative contributions to the total displacement damage from the primary (incoming) protons and the secondary neutrons behind Ta shielding for a particular orbit. Of the secondary particles produced, neutrons are the greatest concern because they penetrate beyond shield depths that stop most primary protons, and yet their interaction cross-sections are significant. Secondary protons produced in nuclear reactions within the shield do not contribute significantly to the device damage since they have short ranges and are stopped in the shield itself. Note that for low atomic number shields such as Al, the displacement damage caused by secondary particles is much less significant. In addition, figure 17 shows that per unit mass, a lower atomic number shield such as Al, minimizes the amount of displacement damage to a CCD [Dale93]. Nevertheless, per unit thickness Ta clearly surpasses Al in shielding efficacy due to it greater density. Since there is generally not the space (or weight budget) to accommodate bulky Al shielding in a satellite application, higher atomic number shields are typically utilized to protect very soft devices.

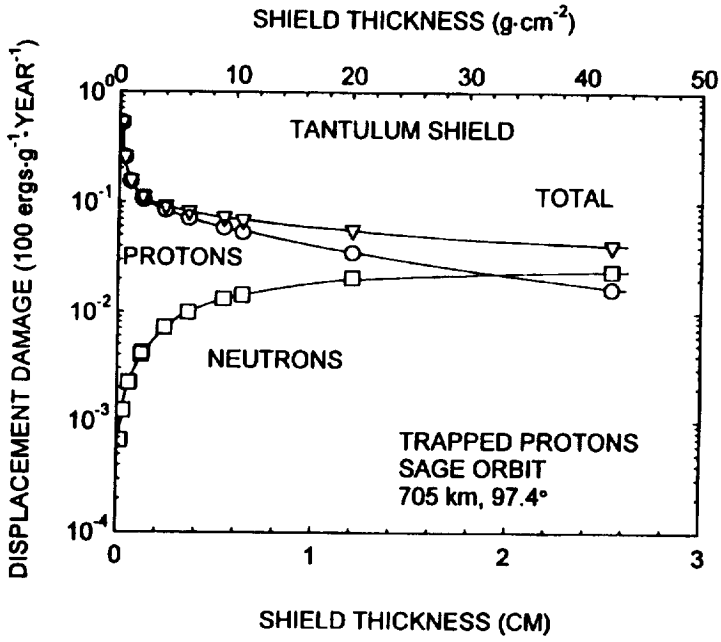

Figure 16 Displacement damage dose behind a Ta shield in a trapped proton environment. Contributions from all protons and secondary neutrons are shown. (The secondary proton dose is negligible.) The secondary neutron dose dominates after about 2 cm Ta. In contrast, for low atomic number material such as Al, secondaries do not contribute significant displacement damage. After [Dale93].

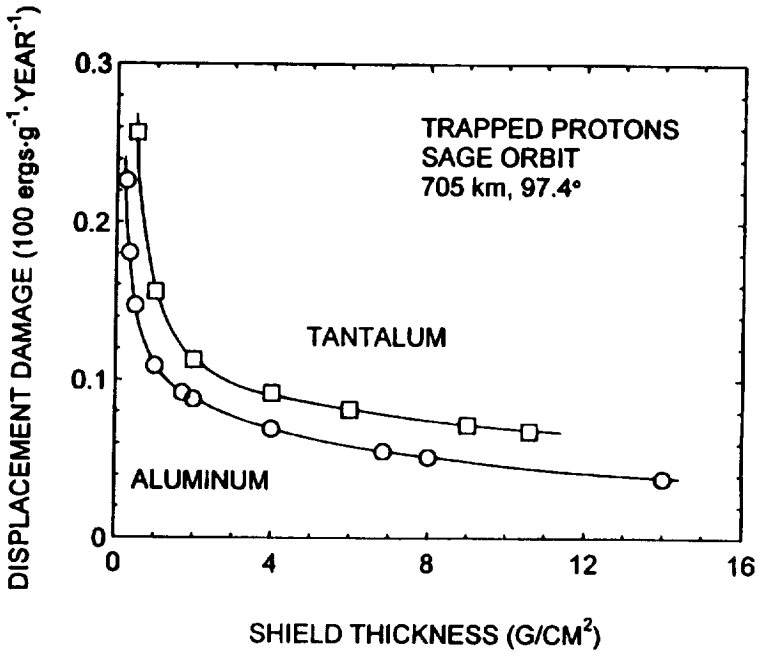

Figure 17 Comparison of displacement damage dose behind Al and Ta shields in density independent units (g/cm^2). Al is the superior displacement damage shield per unit mass. However, since Ta has about six times the density of Al, Ta is always the better shield per unit thickness. After [Dale93].

Perhaps the most difficult (and important) choice facing a radiation effects engineer is which measurement technique to employ in evaluating the proton induced CTE loss. Some of the more commonly used techniques are described in [Hopk96], and references therein. One measurement technique is to plot the intensity and location of well-separated signals produced in the CCD via illumination with X-rays which produce well defined charge packets. X-ray CTE measurements can reproducibly detect very small changes in CTE, but they may considerably over-estimate the CTE degradation that would be observed on-orbit for several reasons. During many missions, CCDs will be viewing scenes that provide significant background radiation charge and larger signal sizes. As seen in figure 15, the CTE in proton irradiated CCDs can be strongly dependent on both signal size and background radiation charge. Also, sophisticated readout algorithms and signal processing software on board the satellite may decrease the impact of CTE loss for a given application. As a simple example, an application may call for the signal in neighboring pixels to averaged together, so that the charge lost to trailing pixels as a result of CTE degradation is less significant. In the case of star tracker applications, the results of X-ray CTE measurements (along with dark current results, etc.), may be input to detailed system level radiation effects models to predict the performance impact. In addition, the irradiated CCDs themselves may be placed in elaborate simulation stations complete with calibrated star fields for a detailed evaluation. However, many satellite applications involve a range of performance requirements, and

less sophisticated laboratory radiation tests must be designed to provide the most reasonable worst case assessment.

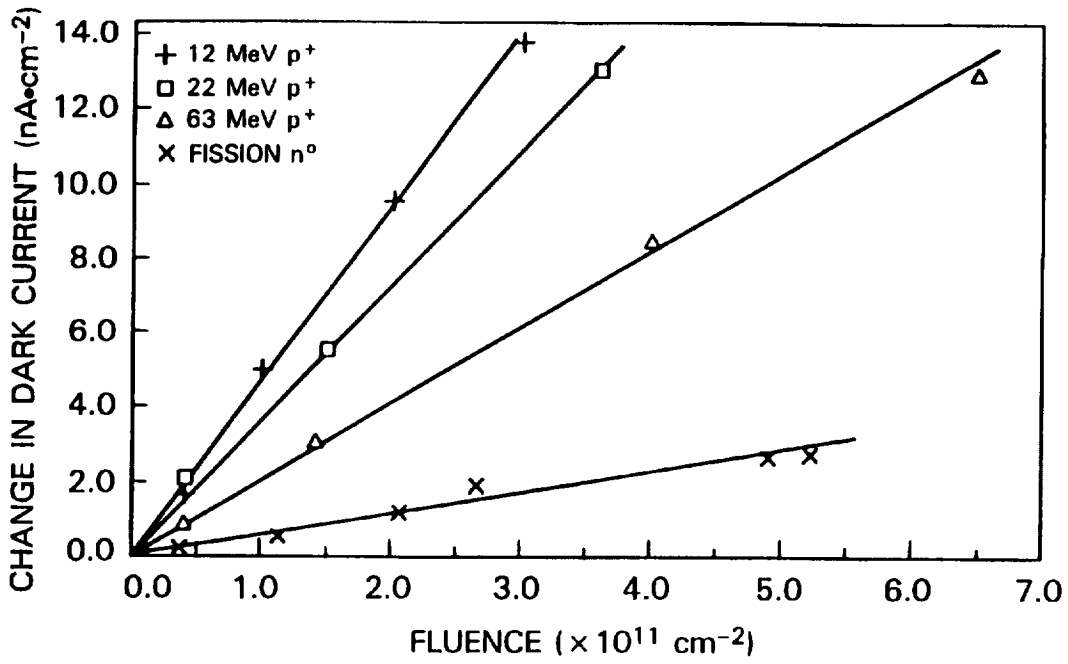

Figure 18 The linear dependence of the change in dark current on particle fluence permits the definition of the dark current damage factor (given by the slopes of the lines). After [Dale89b].

The second major effect of proton induced displacement damage on CCDs is the increase in dark current as a result of carrier generation in the bulk depletion region of the pixel. (This assumes that the CCD or CID has a hardened oxide and/or else is run in inversion so that the surface dark current is suppressed.) The average dark current increase is characterized by a damage factor defined as the change in dark current per unit proton fluence. As shown in figure 18, lower energy protons are more damaging than higher energy protons as expected based on the NIEL energy dependence. (Charge injection devices (CIDs) were used in this study because they have x,y addressable arrays of pixels that are not subject to CTE degradation. These CIDs also had hard oxides.)

Although the increase in the mean dark current with proton irradiation is important, the dark current nonuniformity is generally the biggest concern for CCD applications in space. NIEL is an average quantity just as stopping power (or LET) is an average quantity. For ionization effects, the departure from the average dose delivered in a uniform medium is small down to dimensions measured in hundreds of cubic nanometers. This is not the case with NIEL. For Si detector arrays (such as CIDs or CCDs), with pixels measured in the tens or hundreds of cubic microns, the displacement damage sustained by adjacent pixels can vary considerably even though the identical pixels are exposed to the same environment [Dale89b, Dale90, Mars89b, Mars90]. This nonuniformity is inherent to the statistical nature of the collision kinematics producing the displacement damage and therefore cannot be hardened against.

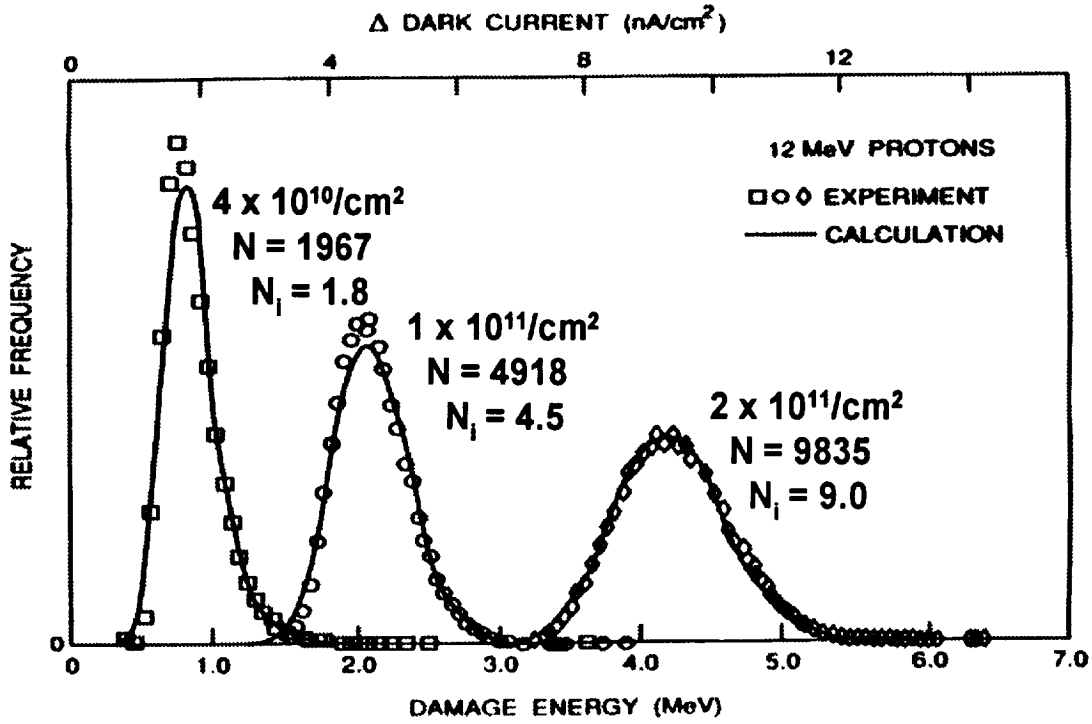

Figure 19 CID dark current histograms after exposure to increasing proton fluences. As the number of primary interactions per pixel, N, increases the distribution approaches a gaussian distribution. The high energy tail is produced by very infrequent but large nuclear reaction events. (N_i is the average number of inelastic interactions per pixel.) After [Mars90 and Dale89b].

Figure 19 illustrates the spread in the dark current increases in individual pixels for a Si CID damaged incrementally by 12 MeV protons. The increase over the pre-irradiation dark current is determined for each pixel and the three histograms are formed from the 61,504 pixel population following each exposure. The high dark current tail is produced from single-particle inelastic nuclear reactions that deposit large amounts of displacement damage energy within the pixel, but are rare enough that relatively few pixels are affected at low fluences. Marshall et al. [Mars89b, Mars90] and Dale et al. [Dale89b, Dale90, Dale94] have studied the statistics of dark current fluctuations in detail and developed quantitative descriptions of the effect. As seen in figure 19, the analytic predictions (solid lines) of the dark current distributions [Mars90] agree well with the experimental results. At higher proton energies, where the primary recoil ranges approach the pixel dimensions, Monte Carlo techniques are required to model the dark current distributions [Dale94]. In some devices, the presence of even very small high electric field regions can result in dark current distributions that are significantly more skewed than those seen in figure 19 [Srou89, Mars89b, Mars90, Dale90, Hopk92]. Improved device design and a reduction of the applied biases can greatly minimize the occurrence of these very high dark current pixels.

The high dark current pixels (so-called spikes) have been observed by several groups in a variety of devices, and also have been noted to have an erratic time

dependence [e.g., Srou86, Hopk89, Mars90, Mill94, Dai96]. Hopkins and Hopkinson showed that the dark current within a single pixel not only fluctuates in time, but also switches between well-defined levels and has the characteristics of random telegraph noise [Hopk92, Hopk93, Hopk95]. This behavior is illustrated in figure 20 for an EEV CCD irradiated by 10 MeV protons. This type of noise represents a significant calibration problem for some applications.

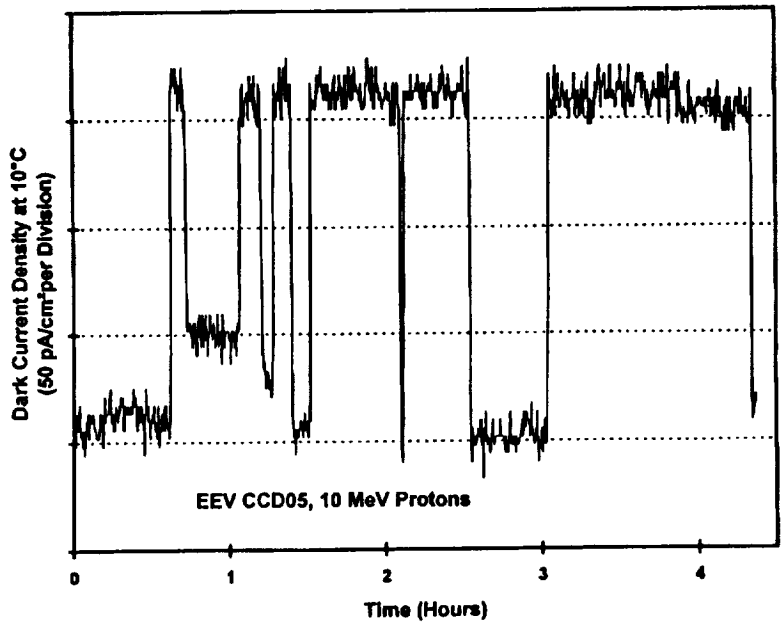

Figure 20 After the proton irradiation of a CCD, some pixels show time fluctuations in the dark current with the appearance of random telegraph noise. These measurements were performed on an EEV imager at 10°C. The mean time constants for the high and low states increased at lower temperatures. After [Hopk93].

Despite the extreme sensitivity of CCDs to displacement damage, they are used successfully in space for many applications. Instrument shielding, CCD cooling, careful selection of device architecture and operating conditions, and signal processing all can be used to partially mitigate the proton induced performance degradation. Other types of two-dimensional sensor arrays, such as photodiode arrays, p-channel CCDs [Spra97] and active pixel sensor arrays show promise for future use in severe space environments.

3.3.3 Photodetectors

Photodetectors are designed to collect photo-generated charge. Since particle-induced charge is also sensed, such devices are inherently radiation sensitive. Displacement damage causes an increase in the bulk dark current via carrier generation in depletion regions. Also, the degradation in minority carrier lifetime (τ) reduces the carrier diffusion length (L) in accordance with the well-known relation, $L = (D\tau)^{1/2}$, where D is the diffusion constant. The result is degradation of the detector responsivity. Nevertheless, adroit selection of components and good system design permits their

successful use in a proton environment. For example in data link and encoder applications, the radiation induced increases in dark current and the reduced responsivity can be accommodated in the optical power link margin [Mars92, Mars94].

The radiation response of many types of detectors has been investigated, including pn junction photodiodes [Soda75, Wicz82, Barn86, Kord89], p-i-n diodes, phototransistors [e.g., Soda75, John96, Reed98], avalanche photodiodes (APDs) [Buch95, Sun97], multi-quantum well infrared photodetectors (MQWIPs) [Khan96], etc. Detectors that depend on the minority carrier lifetime and diffusion limited collection of carriers are much more sensitive to displacement damage than those which do not, such as a fully depleted p-i-n detector [Soda75]. For example, phototransistors are sometimes used as optical detectors (e.g., in optocouplers) since they provide internal gain. However, the transistor gain is dependent on the minority carrier lifetime and therefore sensitive to displacement damage. In contrast, metal-semiconductor-metal (MSM) photodiodes are majority carrier devices and quite robust in a proton environment. As expected, the robustness of a photo-detector also can be very application dependent. Consider an APD that can operate successfully in an analog communications link to the equivalent of 100 krad(Si) in a proton environment, whereas its performance as a photon counting device (in the Geiger mode) significantly degrades for a proton exposure below 100 rad(Si) [Sun97].

Photodiodes are available which are optimized for many applications, and the radiation response is design dependent. For example, one may harden a Si photodiode to displacement damage by minimizing the diffusion limited carrier collection (governed by the minority carrier lifetime), and maximizing collection in the depletion region using lightly doped material. Although such diodes can be quite robust in a proton environment, the lightly doped regions are subject to carrier removal and mobility degradation at relatively low fluences [Kord89]. Note also that sometimes a detector that may be relatively robust to displacement damage, like a fully depleted Si p-i-n, may be relatively more susceptible to ionization induced photo-currents which can produce bit errors in a fiber optic data link. (See Part IVA of the course for a description of bit error effects in fiber links.) Obviously, the radiation response of a particular detector to both permanent and transient proton effects must be considered for a real application.

In recent years, InGaAs p-i-n detectors have proven useful in fiber optic data link applications because of their superior SEE performance as compared to a Si diode [Mars94]. Dark current damage factors were measured as a function of proton energy and were found to agree very well with the calculated InGaAs NIEL [Mars92], as shown in figure 21. The dark current damage factors (and corresponding responsivity damage factors) were combined with proton environment spectra using the formalism presented in section 2.4 to predict the on orbit performance of the detector as a function of orbit altitude and shielding. The dark current results are shown in [Mars92] for a particular orbit. The responsivity results are shown in figure 22 for a wide range of circular orbits. These results further illustrate the breadth of useful results that can be obtained using the displacement damage analysis tools described in this course.

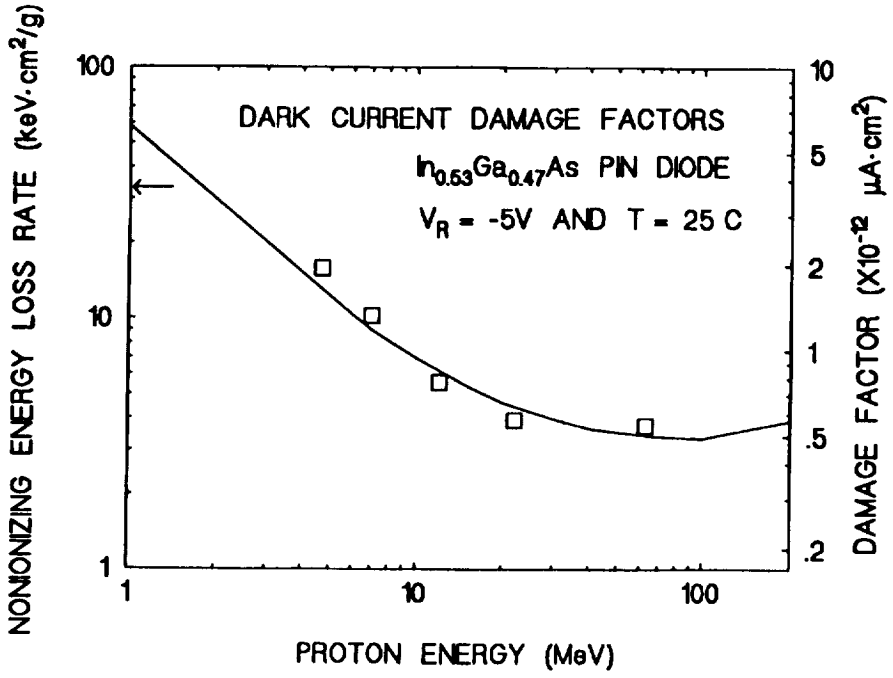

Figure 21 The calculated NIEL for InGaAs exhibits the same energy dependence as measured dark current damage factors. The two are scaled by the constant of $1.4x10^{-10}$ μAg/MeV, which relates device leakage to calculated displacement damage. After [Mars92].

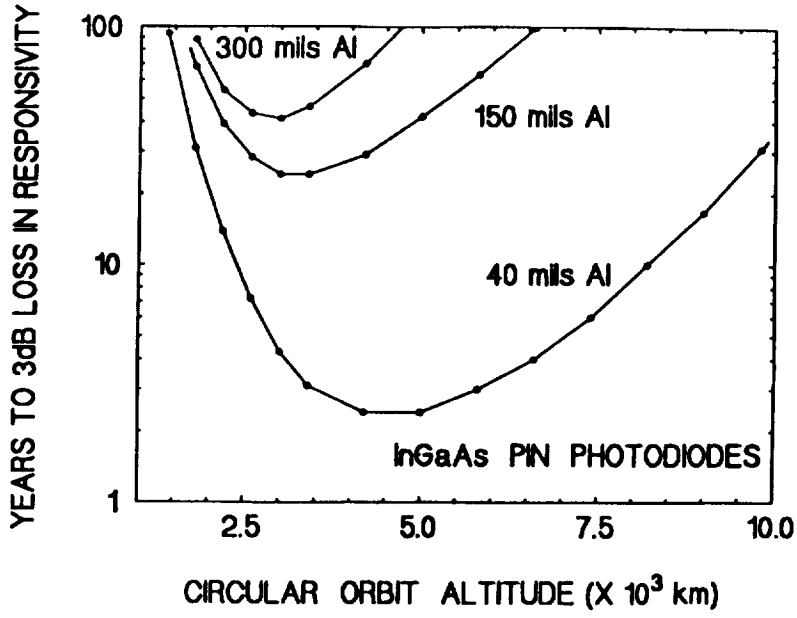

Figure 22 Predicted proton induced responsivity changes for an InGaAs photodiode. Note the shift in the position of the minimum to higher altitudes as the shielding is reduced. This is a

result of the increased low energy component of the proton spectra at higher altitudes, which is stopped in the thicker shields. After [Dale92a].

A recent short course treated radiation effects in infrared (IR) detectors [Pick93]. Additional information can also be found in [Hopk97] and past IEEE Transactions on Nuclear Science (TNS) journals from this conference [e.g., Wate87, Hopk94a]. Very little work on proton effects appears in the open literature, but as new civilian programs (such as NASA's Hubble Space Telescope, Next Generation Space Telescope, ESA's High Resolution Imaging Spectrometer, and others) employ IR sensors this will change. IR sensors are generally fabricated as a hybrid of the IR detector array and a silicon readout circuit, and both elements must be considered. The IR detector elements are sensitive to both TID and, in principle, displacement damage effects, but the materials usually have high enough defect levels to mask proton induced damage to any realistic level expected on-orbit. Even if a linear Si CCD is employed for the readout circuitry, proton displacement damage effects are not generally important. The low operating temperature minimizes dark current and CTE changes, and CTE degradation is also reduced as a result of fast readout rates and relatively high signal levels.

3.3.4 Lasers and Light Emitting Diodes

Photonic subsystems are increasingly widespread on satellite systems because of their performance advantages. Lasers and LEDs are employed in fiber optic communications links [Mars92, LaBe93, Mars94], optocouplers [Rax96, Reed98, Barn98], position encoders, etc. Note that laser modules employed in data links may include both lens and photodiodes, and the radiation response of the passive elements may be significant as discussed in [Mars92, Lisc93].

To date, laser diodes have proven to be relatively insensitive to proton displacement damage effects, even as technology development continues to reduce the threshold currents. Radiation does introduce nonradiative recombination centers that lower the quantum efficiency, resulting in an increased threshold current (and therefore degrades the optical power) [Barnes84]. If the threshold shift is large enough, the laser may fail to operate. Proton measurements on emerging laser technologies such as vertical cavity surface emitting lasers (VCSELs) [Paxt97] and multi-quantum well (MQW) laser diodes [Zhao98, Evan93] demonstrate very robust behavior. As seen in figure 23, MQW lasers exposed to 200 MeV proton fluences of 10^{13} cm^{-2} of (corresponding to almost 1 Mrad(Si) TID), show very minimal degradation [Zhao98]. The current threshold is found to degrade linearly with particle fluence, enabling the definition of a damage constant [Barnes 84].

LEDs are generally more sensitive to proton damage than laser diodes because they tend to have longer minority carrier lifetimes in the light emitting region, and are therefore more sensitive to the introduction of recombination centers [Barnes82, Barnes84]. LEDs may employ different lifetimes in the active volume in order to produce a device with specific qualities such as high light output or high speed, and therefore the resulting radiation sensitivities can be quite different. Although many types

of LEDs are quite robust [Lisc92, Lisc93], amphoterically doped LEDs have been found to be quite sensitive to displacement damage [Barn76, Rose82, Rax96, Barr95, John98].

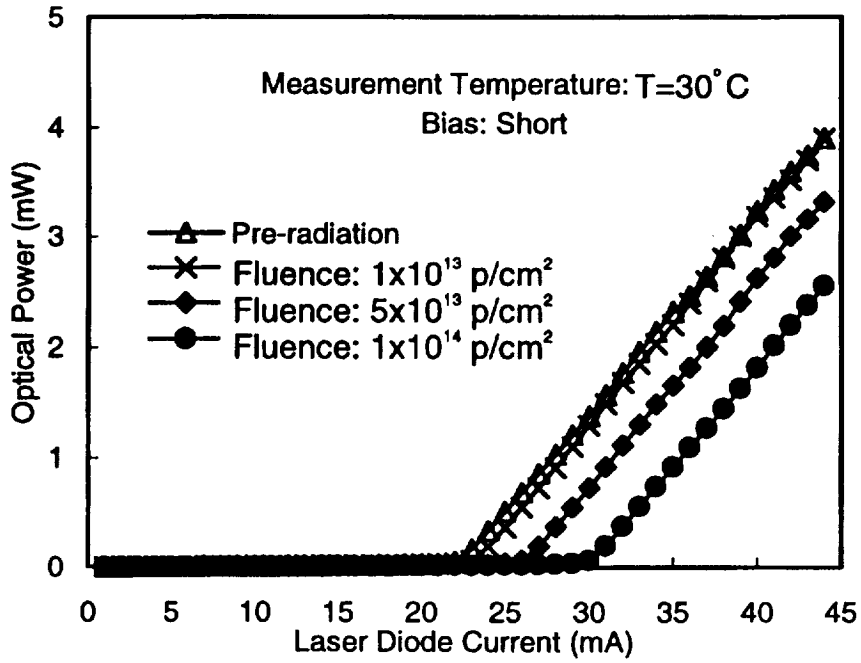

Figure 23 Optical power versus laser drive current for devices shorted during irradiation. The threshold current increases linearly with proton fluence. [After Zhao97].

In fact, such LEDs have been investigated for use as displacement damage monitors on board spacecraft [Barr89, Barr90], as have SiC LEDs [Hinr98]. Recent measurements by Rax et al. have shown that the highly efficient amphoterically doped 890 nm AlGaAs LEDs used in the low speed Optek and Micropac 4N49 optocouplers suffer severe degradation for proton fluences of interest to the satellite community [Rax96]. On the other hand, they found that the shorter wavelength (700 nm) GaAlP heterojunction LED used in the HP 6N140 optocoupler is very resistant to proton damage.

Photonic devices fabricated from compound semiconductors may exhibit forward bias annealing after irradiation. This phenomenon has been observed in laser diodes [Barn70, Mind76, Lisc94, Paxt97, Zhao98] and also in InP solar cells [Ando86, Yama88, Walt91]. It cannot be explained by a rise in the diode junction temperature, and this is generally considered to be due to recombination defect reactions [Lang74, Kime78]. This annealing process is thought to occur as a result of defect motion in response to locally deposited vibrational energy resulting from a non-radiative electronic transition through the defect in a depletion region. Zhao et al. have performed detailed annealing measurements on MQW lasers to characterize the post irradiation annealing of the optical power as a function of forward bias [Zhao 98]. They observed that the degradation in optical power was less at lower proton fluxes as a result of in-situ forward biased annealing during irradiation. This would indicate that tests at laboratory dose rates may over-estimate the degradation that would be observed on-orbit. However, unlike the

complete recovery observed for gamma-irradiated GaAs lasers [Barn70], the lasers exposed to protons have only exhibited a partial optical power recovery [Mind76, Paxt97, Zhao98]. Since various LEDs and laser diodes exhibit different degrees of forward biased annealing, this effect should be characterized for the devices of interest to a specific program. Significant long term annealing at room temperature has not been observed in unbiased devices [e.g., Barr95], as expected.

As discussed in section 2.3.2, care is required in the choice of a damage function for the purpose of performing on-orbit predictions, since the energy dependence of the GaAs NIEL calculation at higher proton energies appears to diverge with recent measurements on GaAs LEDs [Barr95] and MQW lasers [Zhao97]. Depending on the particular proton environment and degree of device shielding, the predicted displacement damage dose can vary by factors of 2-3, (and possibly more) depending on whether the calculation is based on the energy dependence of the calculated NIEL or that of the measured damage factors.

3.3.5 Optocouplers

Optocouplers are hybrid modules comprised of an LED optical source, a coupling medium, and a detector that is sometimes followed by an amplifier stage. They provide the basic function of DC isolation between circuit blocks, and find widespread application on spacecraft. The primary performance metric is the current transfer ratio (CTR), which is the ratio of the photodetector collector current to the LED forward (i.e., drive) current. There are many different optocoupler designs and applications (digital and linear), and the radiation response is highly dependent on both factors. As a result of on-orbit failures of these devices in military and civilian spacecraft, laboratory investigations have been performed that confirm the important role of displacement damage in device degradation. The failure in the TOPEX/Poseidon mission was due to CTR degradation at equivalent TID levels of 10-20 krad(Si) where about 1/3 of the TID was contributed by protons [Rax96]. On-orbit errors may also occur as a result of single event transients (SETs) as discussed in Part IVA of this course. The experience to date has been that SETs are more likely to be an issue for high speed applications (> 1 MHz), whereas displacement damage effects have been most pronounced in optocouplers with a type of LED used in lower speed circuits. Investigations of the radiation response of current optocoupler technology include [Lisc93, John96, DOrd97, Reed98]. To date, optocouplers with amphoterically doped AlGaAs LEDs have displayed the highest sensitivity to proton damage, and modern devices have proved significantly more susceptible than earlier generations [Rose82].

The radiation response of optocouplers is complicated by several factors that have been considered in the recent work cited, and continue to be investigated. First, the devices are hybrid modules that may exhibit large part to part variability. A given commercial hybrid may have internal components (such as LEDs) that cannot be traced and may from several sources. Second, the observed radiation induced degradation results from a combination of TID and displacement damage mechanisms, and the relative importance depends on the optocoupler design and application. Also, the coupler

may be a part of a larger hybrid such as a DC-DC converter, which includes other radiation sensitive components [Reed98]. Third, as described in the previous section, limits in our current understanding of the energy dependence of the NIEL for III-V (and ternary) materials do not permit accurate on-orbit performance predictions, thereby necessitating significant radiation design margins. It is also worthwhile to note that little is known about possible connections between reliability issues such as lifetime and temperature and radiation-induced degradation. Currently, these effects are assumed to be independent. However, we do know that some optocouplers have exhibited a significant CTR temperature dependence, which is an important consideration since operation well above room temperature is not uncommon on spacecraft [Rax96].

The importance of proton testing to evaluate the on-orbit response of an optocoupler is clearly demonstrated in figure 24 which shows greatly decreased CTR for proton as compared to Co-60 irradiation. Rax et al. disassembled two types of optocouplers to investigate the modes of CTR degradation [Rax96]. They found that the CTR performance was primarily determined by the response of the LED to displacement damage, and that the amphoterically doped AlGaAs LED was significantly more susceptible than the GaAlP LED. As is often the case, a higher performance device fabricated with more pristine material is also more radiation sensitive (e.g., CCDs, solar cells, etc.), and an engineering trade of initial performance versus the radiation sensitivity of the device on-orbit must be performed. Displacement damage also affected the phototransistors in each optocoupler studied by Rax et al., with the reduction in photoresponse being a more significant than gain degradation. Optocouplers that use a photodiode (as opposed to a phototransistor) have been observed to have the best performance to date [Reed98].

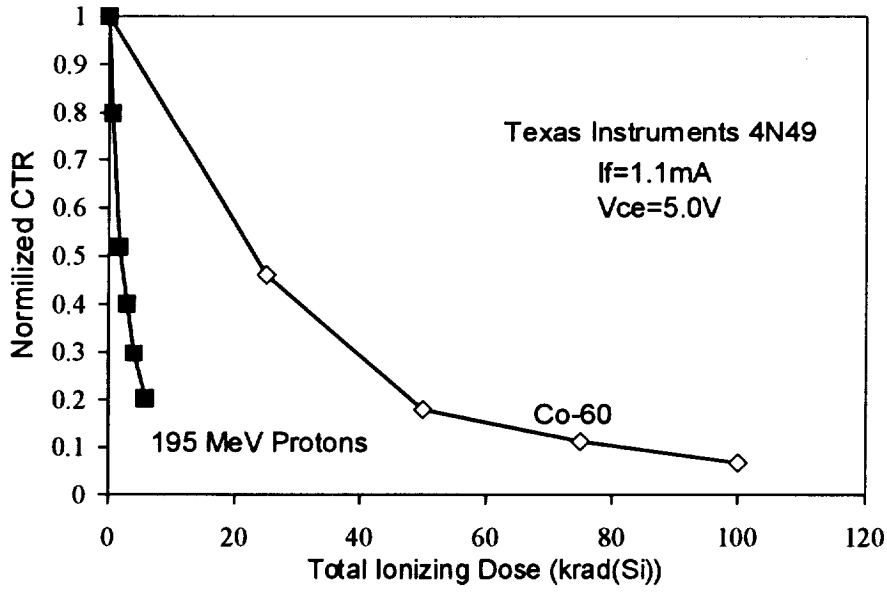

Figure 24 Comparison of proton and gamma irradiations clearly demonstrates the importance of displacement damage in CTR degradation. Despite the large part to part variability in the pre-

irradiation CTR values, similar radiation degradation is observed when the post-irradiation CTRs were normalized to their initial values [Rax98]. After [Reed98].

Application specific laboratory testing is necessary in order to assess on-orbit CTR performance. To begin, we note there is a distinct difference in the performance and electrical characteristics of general purpose optocouplers, such as those evaluated in [Lisc93, Rax96, Reed98] and those used in linear applications, e.g., DC-DC converters. General purpose devices exhibit a wide range of CTR values guaranteed to be above a set minimum, whereas those in linear applications have specified CTRs within a narrow range. These differences need to be considered in designing a laboratory evaluation to determine the suitability of such devices for use in space [John99]. In all cases, a proton induced radiation response of an optocoupler will depend on the LED drive current since it impacts the operating point of the phototransistor and therefore, its radiation response.

The importance of application specific testing has been demonstrated by Reed et al. in a study that measured the impact of LED drive current, circuit loading, and the phototransistor collector-emitter voltage (V_{CE}) on the proton induced CTR degradation. The experimental set-up is illustrated in figure 25. A radiation induced degradation in the LED light output results in a reduction in the collector current of the phototransistor. If the transistor is in saturation then the change in collector current will be minimal and the CTR will be essentially the same. However, if the same device is operating in the active region, the CTR will be quite sensitive to changes in LED output power. Whether or not the transistor operates in saturation is dependent on the LED drive current and V_{CE}, (which itself depends on the output load). Figure 26 illustrates the load dependence of the CTR radiation response for an optocoupler operated with a forward current of 4 mA. It also demonstrates that the common practice of testing at a fixed V_{CE} of 5 V with no circuit loading significantly over-predicts the CTR degradation, although such data can be used for worst case estimates. Data such as these suggest the mitigation of CTR degradation by operation of the optocoupler at the highest drive current possible while minimizing V_{CE} to obtain the desired I_C for the application [Reed98]. In this case the optocoupler is driven into saturation. However, the trade-off between reliability concerns for LED operation in this mode must be considered. Also, the forward current selected may impact the rate of defect annealing observed in some LEDs, as discussed in the previous section.

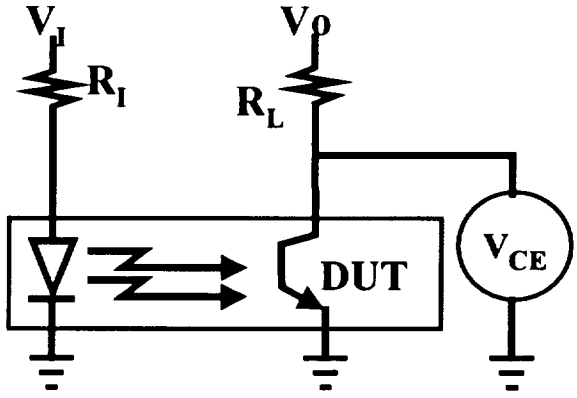

Figure 25 CTR measurement setup showing the input voltage and resistance (V_I and R_I), and output voltage (V_O). Two independent power supplies are used to sweep V_I and V_O. Changes in

V_I alter the LED drive current. V_{CE} is the difference between V_O and the measured voltage drop across the load resistance (R_L), which can be varied. After [Reed98].

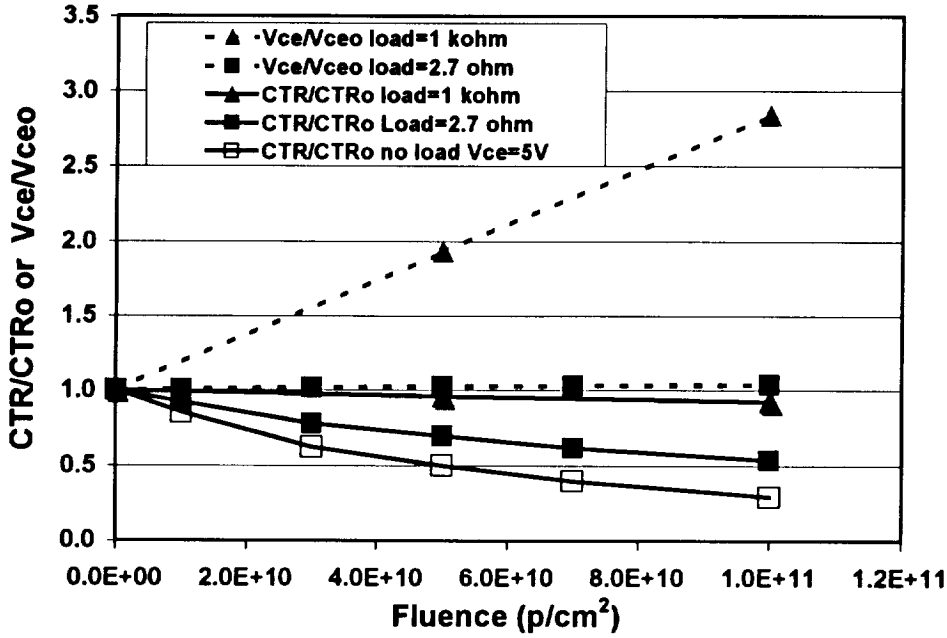

Figure 26 Plot of the normalized CTR (solid lines) and normalized V_{CE} (dashed lines) for an optocoupler operated with a forward current of 4 mA and irradiated with 195 MeV protons. In the case of the 2.7 Ω load (with V_{CE} remaining at 0.3 V), the degradation is almost twice that observed for the 1 kΩ load where the degradation is mitigated by an increase in V_{CE}. (V_o was set so that the initial V_{CE} = 0.3 V for both loads.) After [Reed98].

To the extent that laboratory testing has shown the CTR response to be dominated by displacement damage to the internal LED, the analysis tools presented in sections 2.3 and 2.4 can be used together with application specific CTR measurements on proton-irradiated devices to perform on-orbit predictions. As always, it is important to select the optimal proton test energy (or energies) based on analysis of the shielded proton spectrum relevant to a specific application. The relative importance of displacement damage dose and TID may be assessed by comparing proton and gamma measurements as indicated in figure 24. This figure also shows that the CTR response is very nonlinear with proton fluence (or TID or displacement damage dose), so that a damage factor cannot be defined. Nevertheless, the CTR degradation can be plotted versus the equivalent mission fluence or displacement damage dose to assess the end of life performance. (Note that, to first order, the proton testing of CTR degradation can also be considered to incorporate the performance loss from TID effects.) As noted in the previous section, the NIEL function for LED materials does not accurately reflect the device response so accurate predictions are not presently possible. In the absence of CTR measurements as a function of proton energy, we have three choices for a function to describe the energy dependence: (1) a calculated NIEL curve, (2) an experimental displacement damage curve from the literature (e.g., the LED data from [Barr95]), and (3) a piecewise "manufactured" worse case damage function. It is hoped that further research to permit a better understanding of the radiation performance of optocouplers

and the applicability of the NIEL energy dependence will result in more realistic worst case analyses to facilitate the device selection process. However, there will still remain a wide variation between optocoupler manufacturers concerning issues such as component procurement and coupler design. These issues need to be reflected in the sample size chosen for a radiation test, and significant de-ratings may be necessary to reflect the large part-to-part variations observed for some of these hybrid devices.

3.3.6 Solar Cells

Solar cells are basically very specialized large area diodes, some of which have complex multi-junction designs to optimize their conversion efficiency. Light strikes the solar cell and creates electron-hole pairs that generate electrical power only if collected at the cell electrodes. In order to have high collection efficiency, especially at the red end of the spectrum, long diffusion lengths are required in the lightly doped portion of the cells intended for light collection. As expected for a minority carrier device, the degradation in power output is a result of a radiation induced reduction in the minority carrier lifetime. Once again, device radiation sensitivity is greater for materials with longer initial lifetimes, as seen in figure 27. For example, minority carrier lifetimes in GaAs are typically much shorter (tens of nanoseconds) as compared to the much longer Si lifetimes of tens to even hundreds of microseconds. Key electrical parameters include not only the power output, but also the open circuit voltage, and short circuit current. The interested reader may find a wealth of information in the JPL solar cell handbooks [Tada82, Ansp89, Ansp96], and the Photovoltaic Specialists Conference proceedings.

Crystalline Si and GaAs/Ge solar cells are most commonly flown today, but multi-junction GaAs cells, InP and amorphous Si cells are being investigated for future use in space. The drive to fly spacecraft in ever more harsh environments (including the more intense part of the proton belts) has spurred interest in more radiation hardened cells. The presence of multiple junctions provides additional design flexibility to achieve increased hardness, as described in [Marv99]. Figure 27 compares the maximum power output degradation as a function of displacement damage dose for several of the most common solar cell materials. The figure summarizes data from several sources [Srou98, Wojt96, Mess97, Hoff97, Nogu90], and clearly shows the nonlinear degradation. Note that InP has the potential for increased survivability as a result of injection annealing [Keav93]. However, as noted in the case of GaAs LEDs and laser diodes, the degree of annealing characteristic of a particular device needs to be carefully confirmed in a well designed ground test of the flight lot. Note that the amorphous Si cell has been shown by Srour et al. to degrade primarily by TID effects, which is not surprising due to the disordered nature of the material [Srou98].

At very high fluences, minority carrier devices begin to show the effects of carrier removal, and solar cells are no exception. The rapid degradation of solar cell output power at high displacement damage doses illustrated in figure 27 and is due to carrier removal. In fact, failure of a Si solar cell flown in an elliptical orbit through the Van Allen belts from carrier removal effects has been observed [Yama96, Amek97]. Recent

work by Messenger et al. has investigated the response of InP solar cells to high proton fluences (including carrier removal effects) [Mess97a, Mess98].

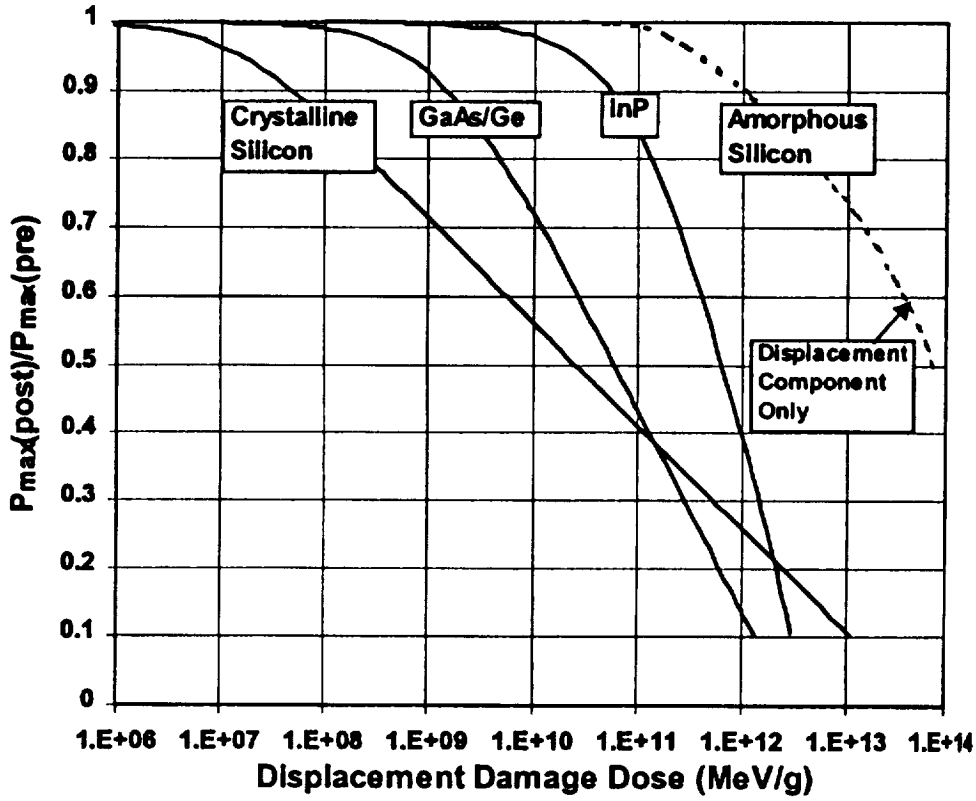

Figure 27 Maximum power output degradation versus displacement damage dose for a variety of solar cells. The amorphous Si curve includes the displacement component only, and does not include ionization induced degradation. After [Srou98].

Since solar cell performance degrades as a result of displacement damage the analysis tools presented in sections 2.3 and 2.4 can be applied to perform on-orbit predictions. For example, these techniques have been used to predict the on-orbit power degradation of GaAs solar cells due to a solar proton event [Mess97b]. Since these devices are flown in space with very thin shielding (e.g., coverglasses as thin as 3 mil), the lower energy portion of the proton spectrum contributes the bulk of the displacement damage. Note that the deviations of the damage factors from the GaAs NIEL dependence (see figure 9) are less significant in performing a solar cell analysis because the measurements are fit to the NIEL calculation over a much smaller energy range. For the case of a 3 mil SiO_2 coverglass, less than 10% of the total displacement damage dose calculated for the 1989 solar flare event is contributed by protons with energies greater than 12 MeV [Mess97b]. Clearly, proton test energies should be chosen accordingly, with care taken to ensure the NIEL is not varying significantly as the particle transverses the device under test (see section 3.2).

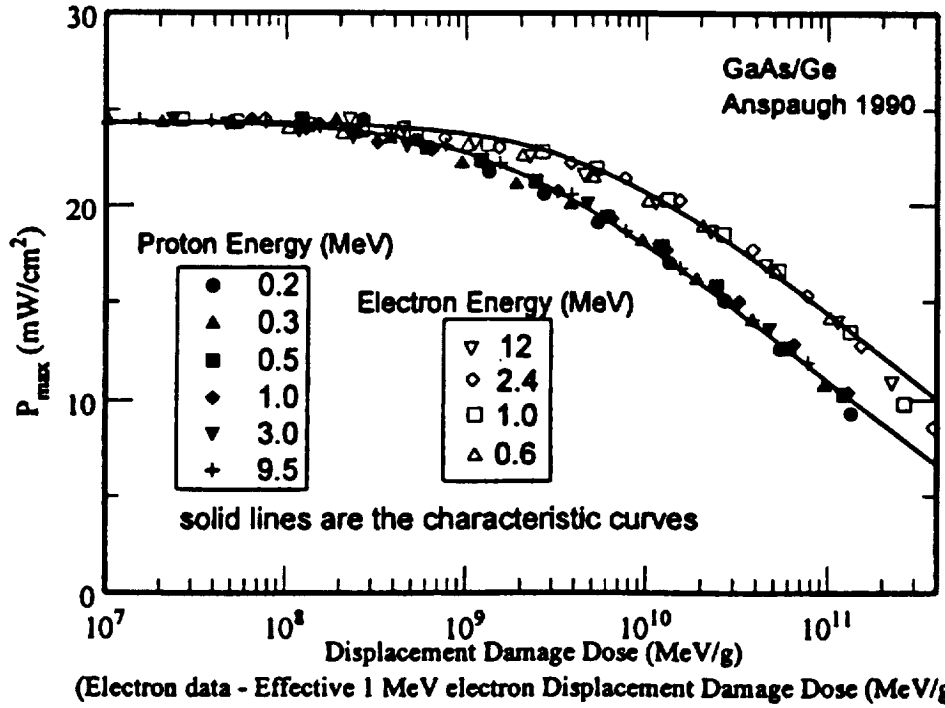

Figure 28 Although the maximum power output correlates well with NIEL over the proton energy range shown, the electron fit was obtained by defining the equivalent 1 MeV electron displacement damage dose as the product of the particle fluence with NIEL raised to the 1.7 power. After [Walt99].

The light shielding employed in solar cells applications has another important consequence. Displacement damage from electrons must be considered in addition to the proton contribution. It has been long recognized that a linear relationship between electron damage factors and NIEL is not always observed in Si [Cart66]. In the case of GaAs solar cells, Summers et al. [Summ93] presented short circuit current data showing a "nearly" linear relationship (on a log-log plot) between both the electron and proton data and the calculated GaAs NIEL using data from [Ansp92]. (Many of the correlations of calculated NIEL with device performance discussed in section 2.3 were initially presented on log-log plots covering many orders of magnitude, which makes it difficult to assess the degree of linearity where factors of 2-3 are significant.) More recently, Walters et al. [Walt99] have performed a detailed review of the above-mentioned GaAs data set, and now recommend separate fits to the NIEL in order to describe proton and electron degradation. The fits are shown in figure 28, and we see the proton data correlate well with NIEL *over the energy range from 0.2 to 9.5 MeV*. For electrons, they find that the best agreement of the data over the largest energy range is obtained when the calculated NIEL was raised to the 1.7 power. As a result, they define the equivalent 1 MeV electron displacement damage dose as the product of the particle fluence with NIEL raised to the 1.7 power. This example illustrates one method of modifying the NIEL correlation in order to perform an on-orbit prediction for a quantity that does not exhibit the energy dependence predicted by NIEL. Obviously, other fitting approaches can also be employed to describe the measured device degradation after irradiation, and all require measurements of the device degradation for a set of particle energies.

4.0 SUMMARY

Section IVB begins by examining the process by which incident protons displace atoms in semiconductor material and ultimately produce electrically active defect levels. The impact of displacement damage induced defects on the operation of semiconductor devices is described. In general, devices whose primary characteristics depend on the minority carrier lifetime will be most sensitive to displacement damage. The concept of the non-ionizing energy loss rate (NIEL) is introduced, and it is shown that in many cases device degradation as a function of proton energy is approximately linearly dependent on the NIEL for a variety of materials. This means that the NIEL is the displacement damage equivalent of the LET for total ionizing dose effects. We present displacement damage tools (based on NIEL or experimental damage functions) that allow on-orbit prediction of device degradation based on a small number of laboratory measurements. Limitations in the application of NIEL are also discussed. We find that experimental data for Si and GaAs devices show that NIEL overpredicts device degradation at higher proton energies.

Finally, we presented a series of case studies that illustrate the displacement damage concepts and analysis tools covered in the first part of section IVB. Laboratory radiation test issues specific to the proper evaluation of devices for displacement damage effects are treated. The response of several categories of devices to protons, including bipolar transistors, charge transfer devices, photo-detectors, solar cells, lasers and LEDs are described. Each case study brings to light a new aspect of displacement damage analysis. Si linear bipolar technology exhibits a wide range of displacement damage sensitivity depending on the process, IC design and application. For both Si and SiGe devices, the lateral pnp transistor exhibits an enhanced sensitivity to both TID and displacement damage. The response of CCDs to protons is unique for several reasons. The CTE degradation is determined by the interplay between the carrier emission and capture dynamics of the radiation induced traps and the device readout scheme and clocking rates. Although the increase in the mean dark current with proton irradiation is important, the dark current nonuniformity is generally the biggest concern for CCD applications in space. Dark current within a single pixel are also found to fluctuate in time in a manner characteristic of random telegraph noise. Finally, even when available mitigation techniques are employed, CCDs remain quite sensitive to proton induced damage so that thick, high atomic number shielding is frequently employed on-orbit. We found that predictions of device performance in space must consider the displacement damage produced both by incident protons and secondary neutrons produced in the thick shielding. At the other extreme, solar cells are flown with minimal shielding and therefore lower energy protons are most important and electron damage must also be considered. Photo-detectors are inherently sensitive to radiation but such devices also exhibit a wide range of proton sensitivity dependent on their design and application. Although lasers are generally quite hard to displacement damage, certain types of LEDs exhibit significant loss in output power after low levels of proton exposure. Optocouplers also have a wide range of sensitivities to protons dependent on their design, type of LED used and application. As hybrid devices, they also present significant hardness assurance challenges. In all cases, the device response to proton irradiation is found to be very application dependent, which must be reflected in the design of laboratory radiation tests.

5.0 ACKNOWLEDGMENTS

The authors appreciate the consistent support and friendship of colleagues at NASA-GSFC, NRL and elsewhere. Over the years, we have benefited tremendously from technical interchange with Ken LaBel, Robert Reed and Janet Barth. We have enjoyed working with Ed Burke and Al Wolicki on displacement damage issues. They have been an inspiration, and also patient teachers. Martha O'Bryan was indispensable on several fronts including graphics support.

6.0 REFERENCES

(All references are unclassified.)

[Alur91] M. Alurralde, M. Victoria, A. Caro, and D. Gavillet, "Nuclear and Damage Effects in Si Produced by Irradiations with Medium Energy Protons," IEEE Trans. Nucl. Sci., Vol. 38, No. 6, pp. 1210-1215, 1991.

[Amek97] H. Amekura, N. Kishimoto, and K. Kono, "Radiation-Induced Two-Step Degradation of Si Photoconductors and Space Solar Cells," RADECS97, IEEE Doc. No. 97TH8294, pp. 376-381, 1997.

[Ando86] K. Ando, M. Yamaguchi, and C. Uemura, "Non-Radiative-Recombination-Enhanced Defect-Structure Transformation in Low Temperature Gamma-Ray-Irradiated InP," Phys. Rev. B. Vol. 34, p. 3041, 1986.

[Ansp92] B.E. Anspaugh, "Proton and Electron Damage Coefficients for GaAs/Ge Solar Cells," Proceedings of the 22nd IEEE Photovoltaic Specialists Conference, pp. 1593-1598, 1992.

[Ansp89] B.E. Anspaugh, Solar Cell Radiation Handbook, JPL Publication 82-69, Addendum 1, 1989.

[Ansp96] B.E. Anspaugh, GaAs Solar Cell Handbook, JPL Publication 96-9, 1996.

[Arim82] I. Arimura and C.E. Barnes, "Proton Damage in Laser Diodes and Light-Emitting Diodes (LEDs)," Proc. SPIE, Vol. 328, pp. 83-87, 1982.

[Aver83] R.S. Averbach, R. Benedek, K.L. Merkle, "Ion-Irradiation Studies of the Damage Function of Copper and Silver," Phys. Rev. B18, pp. 4156-4171, 1978.

[Aver88] R.S. Averbach and T. Diaz de la Rubia, "Dynamics and Structure of Energetic Displacement Cascades," Nucl. Instr. Meth. in Phys. Res., Vol. B33, pp. 693-699, 1988.

[Bang91] E.K. Banghart, J.P. Lavine, E.A. Trabka, E.T. Nelson, and B.C. Burkey, "A Model for Charge Transfer in Buried-Channel-Charge-Coupled Devices at Low Temperatures," IEEE Trans. Elect. Dev., Vol. 38, No. 5, pp. 1162-1173, 1991.

(All references are unclassified.)

[Barn70] C.E. Barnes, "Effects of Co^{60} Gamma Irradiation on Epitaxial GaAs Laser Diodes," Phys. Rev. B, Vol. 1, No. 12, 1970.

[Barn84] C.E. Barnes and J.J. Wiczer, "Radiation Effects in Optoelectronic Devices," Sandia Report SAND-0771, Sandia National Laboratories, May 1984.

[Barn86] C.E. Barnes, "The Effects of Radiation on Optoelectronic Devices," Proc. SPIE, Vol. 721, pp. 18-25, 1986.

[Barr89] A.L. Barry, R. Wojcik, and A.L. MacDiarmid, "Response of GaAs Displacement Damage Monitors to Protons, Electrons, and Gamma Radiation," IEEE Trans. Nucl. Sci., Vol. 36, No. 6, pp. 2400-2404, 1989.

[Barr90] A.L. Barry, R. Maxseiner, R. Wojcik, M.A. Briere, and D. Braunig, "An Improved Displacement Damage Monitor," IEEE Trans. Nucl. Sci., Vol. 37, No. 6, pp. 1726-1731, 1990.

[Barr95] A.L. Barry, A.J. Houdayer, P.F. Hinrichsen, W.G. Letourneau, and J. Vincent, "The Energy Dependence of Lifetime Damage Constants in GaAs LEDs for 1-500 MeV Protons," IEEE Trans. Nucl. Sci., Vol. 42, No. 6, pp. 2104-2107, 1995.

[Bert68] M. Bertolotti, "Radiation Effects in Semiconductors," Proceedings of the Santa Fe Conference, edited by F.L. Vook, Plenum Press, NY, p. 311, 1968.

[Burk86] E.A. Burke, "Energy Dependence of Proton-Induced Displacement Damage in Silicon," IEEE Trans. Nucl. Sci., Vol. 33, No. 6, pp. 1276-1281, 1986.

[Burk91] B. Burke and S.A. Gajar, "Dynamic Suppression of Interface-State Dark Current in Buried Channel CCD Imagers," IEEE Elect. Dev. Lett., Vol. 38, No. 2, pp. 285-290, 1991.

[Buch95] F. Buchinger, A. Kyle, J.K.P. Lee, C. Webb, and H. Dautet, "Identification of Individual Bistable Defects in Avalanche Photodiodes," Appl. Phys. Lett., Vol. 66, No. 18, pp. 2367-2369, 1995.

[Carb93] J. Carbone, J. Zamowski, F. Arnold, and J. Hutton, "New Low-Noise Random Access, Radiation Resistant and Large Format Charge Injection Device (CID) Imagers," Proc. SPIE, Vol. 1900, pp. 170-180, 1994.

[Cart66] J.R. Carter, "Effect of Electron Energy on Defect Introduction in Silicon," J. Phys. Chem. Solids, Vol. 27, pp. 913-918, 1966.

[Dai96] M. Dai, F. Buchinger, J.K.P. Lee, and H. Dautet, "Time Resolved Annealing Studies of Single Neutron Irradiated Avalanche Photodiodes," IEEE Trans. Nucl. Sci., Vol. 44, No. 6, pp. 2595-2600, 1996.

[Dale88] C.J. Dale, P.W. Marshall, E.A. Burke, G.P. Summers, and E.A. Wolicki, "High Energy Electron Induced Displacement Damage in Silicon," IEEE Trans. Nucl. Sci., NS-35, pp. 1208-1214, 1988.

(All references are unclassified.)

[Dale89a] C.J. Dale, P.W. Marshall, G.P. Summers, E.A. Wolicki, and E.A. Burke, "Displacement Damage Equivalent to Dose in Silicon Devices," Appl. Phys. Lett., Vol. 54, No. 5, p. 451, 1988.

[Dale89b] C.J. Dale, P.W. Marshall, E.A. Burke, G.P. Summers, and G.E. Bender, "The Generation Lifetime Damage Constant and its Variance," IEEE Trans. Nucl. Sci., Vol. 36, No. 6, pp. 1872-1881, 1989.

[Dale90] C.J. Dale, P.W. Marshall, and E.A. Burke, "Particle-Induced Spatial Dark Current Fluctuations in Focal Plane Arrays," IEEE Trans. Nucl. Sci., Vol. 37, No. 6, pp. 1784-1793, 1990.

[Dale91] C.J. Dale and P.W. Marshall, "Displacement Damage in Silicon Imagers for Space Applications," Proc. SPIE, Vol. 1447, pp. 70-86, 1991.

[Dale92a] C.J. Dale and P.W. Marshall, "Radiation Response of 1300 nm Optoelectronic Components in a Natural Space Radiation Environment," Proc. SPIE, Vol. 1791, pp. 224-232, 1992.

[Dale92b] C.J. Dale, P.W. Marshall, B. Cummings, L. Shamey, R. Howard, and A. Delamere, "Spacecraft Displacement Damage Dose Calculations for Shielded CCDs," Proc. SPIE, Vol. 1656, pp. 476-487, 1992.

[Dale93] C.J. Dale, P.W Marshall, B. Cummings, L. Shamey and A. Holland, "Displacement Damage Effects in Mixed Particle Environments for Shielded Spacecraft CCDs", IEEE Trans. Nucl. Sci., Vol. 40, No. 6, pp. 1628-1637, 1993.

[Dale94] C.J. Dale, L. Chen, P.J. McNulty, P.W. Marshall, and E.A Burke, "A Comparison of Monte Carlo and Analytic Treatments of Displacement Damage in Microvolumes," IEEE Trans. Nucl. Sci., Vol. 41, No. 6, pp. 1974-1983, 1994.

[DOrd97] M.D. D'Ordine, "Proton Displacement Damage in Optoelectronic Devices," 1997 IEEE Radiation Effects Workshop Record, IEEE No. 97TH8293, pp. 122-124, 1997.

[Eise92] F.H. Eisen, K. Bachem, E. Klausman, K. Koehler, and R. Haddad, "Ion Irradiation Damage in n-Type GaAs in Comparison with its Electron Irradiation Damage," J. Appl. Phys., Vol. 72, No. 12, pp. 5593-5601, 1992.

[Gaut83] M.K. Gauthier and D.K. Nichols, "A Comparison of Radiation Damage in Linear ICs from Cobalt-60 Gamma Rays and 2.2 MeV Electrons," IEEE Trans. Nucl. Sci., No. 6, pp. 4192-4196, 1983.

[Gove84] J.E. Gover and J.R. Srour, "Basic Radiation Effects in Nuclear Power Electronics Industry," Sandia Report SAND-85-0776, Sandia National Laboratories, May 1985.

[Grif91] P.J. Griffin, J.G. Kelly, T.F. Luera, A.L. Barry, and M.S. Lazo, "Neutron Damage Equivalence in GaAs," IEEE Trans. Nucl. Sci., Vol. 38, No. 6, pp. 1216-1224, 1991.

(All references are unclassified.)

[Hash94] G.L. Hash, J.R. Schwank, M.R. Shaneyfelt, C.E. Sandoval, M.P. Connors, T.J. Sheridan, F.W. Sexton, E.M. Slayton, J.A. Heise, and C.C. Foster, "Proton Irradiation Effects on Advanced Digital and Microwave III-V Components," IEEE Trans. Nucl. Sci., Vol. 41, No. 6, pp. 2259-2266, 1994.

[Hein83] H.L. Heinisch, "Defect Production in Simulated Cascades: Cascade Quenching and Short Term Annealing," J. Nucl. Mater., Vol. 117, pp. 46-54, 1983.

[Hinr98] P.F. Hinrichsen, A.J. Houdayer, A.L. Barry, and J. Vincent, "Proton Induced Damage in SiC Light Emitting Diodes," IEEE Trans. Nucl. Sci., Vol. 45, No. 6, pp. 2808-2812, 1998.

[Hoff97] R.W. Hoffman, Jr., N.S. Fatemi, P.P. Jenkins, V.G. Weizer, M.A. Stan, S.A. Ringel, D.A. Scheiman, D.M. Wilt, D.J. Brinker, R.J. Walters, and S.R. Messenger, "Improved Performance of p/n InP Solar Cells," Record of 26th IEEE Photovoltaic Specialists Conference, IEEE Catalog No. 97CB36026, pp. 815-818, 1997.

[Holl91a] A.D. Holland, "Annealing of Proton-Induced Displacement Damage in CCDs for Space Use," Inst. Phys. Conf. Ser. 121, pp. 33-40, Sept. 1991.

[Holl91b] A. Holland, A. Holmes-Seidle, B. Johlander, and L. Adams, "Techniques for Minimizing Space Proton Damage in Scientific Charge Coupled Devices," Trans. Nucl. Sci., Vol. 38, No. 6, pp. 1663-1670, 1991.

[Holm93] A. Holmes-Seidle and L. Adams, A Handbook of Radiation Effects, Oxford University Press, Oxford, 1993.

[Hopk89] G.R. Hopkinson and Ch. Chlebek, "Proton Damage Effects in an EEV CCD Imager," IEEE Trans. Nucl. Sci., Vol. 36, No. 6, pp. 1865-1871, 1989.

[Hopk92] G.R. Hopkinson, "Cobalt-60 and Proton Radiation Effects on Large Format, 2-D, CCD Arrays for an Earth Imaging Application," IEEE Trans. Nucl. Sci., Vol. 39, No. 6, pp. 2018-2025, 1992.

[Hopk93] I.H. Hopkins and G.R. Hopkinson, "Random Telegraph Signals from Proton-Irradiated CCDs," IEEE Trans. Nucl. Sci., Vol. 40, No. 6, pp. 1567-1574, 1993.

[Hopk94a] G.R. Hopkinson, C.J. Baddiley, D.R.P. Guy, and J.E. Parsons, "Total Dose and Proton Testing of a Commercial HgCdTe Array," IEEE Trans. Nucl. Sci., Vol. 41, No. 6, pp. 1966-1973, 1994.

[Hopk94b] I.H. Hopkins, G.R. Hopkinson, and B. Johlander, "Proton-Induced Charge Transfer Degradation in CCDs for Near-Room Temperature Applications," IEEE Trans. Nucl. Sci., Vol. 41, No. 6, pp. 1984-1990, 1994.

[Hopk95] I.H. Hopkins and G.R. Hopkinson, "Further Measurements of Random Telegraph Signals in Proton-Irradiated CCDs," IEEE Trans. Nucl. Sci., Vol. 42, No. 6, pp. 2074-2081, 1995.

(All references are unclassified.)

[Hopk96] G.R. Hopkinson, C.J. Dale, and P.W. Marshall, "Proton Effects in Charge-Coupled Devices," IEEE Trans. Nucl. Sci., Vol. 43, No. 2, pp. 614-627, 1996.

[Hopk97] G.R. Hopkinson, "Radiation Effects in Optoelectronic Components," 4th European Conference on Radiations and their Effects on Components and Systems (RADECS 97) Journal of Technical Events, pp. III 65-101, Cannes, France, 1977.

[Jane95] J. Janesick, T. Elliott, R. Winzenread, J. Pinter, and R. Dyck, "Sandbox CCDs," Proc. SPIE, Vol. 2415, pp. 2-42, 1995.

[John87] A.H. Johnston and R.E. Plaag, "Models for Total Dose Degradation of Linear Integrated Circuits," IEEE Trans. Nucl. Sci., Vol. 34, No. 6, pp. 1474-1480, 1987. *{Note that this paper also treats displacement damage.}*

[John99] A. H. Johnston and B.G. Rax, "Proton Damage in Linear and Digital Optocouplers," to be presented at RADECS99 and published in the proceedings.

[Keav93] C.J. Keavney, R.J. Walters and P.J. Drevinsky, "Optimizing the Radiation Resistance of InP Solar Cells: Effect of Dopant Density and Cell Thickness," J. Appl. Phys., Vol. 73, pp. 60-70, 1993.

[Khan96] S.M. Khanna, H.C. Liu, P.H. Wilson, L. Li, and M. Buchanan, "High Energy Proton and Alpha Radiation Effects on GaAs/AlGaAs Quantum Well Infrared Photodetectors," IEEE Trans. Nucl. Sci., Vol. 43, No. 6, pp. 3012-3018, 1996.

[Kim79] L.C. Kimerling, P. Blood, and W.M. Gibson, "Defect States in Proton-Bombarded Silicon at T<300K," International Conf. on Defects and Radiation Effects in Semiconductors, Inst. Phys. Conf. Ser. 46, pp. 273-280, 1979.

[Kord89] R. Korde, A. Ojha, R. Braasch, and T.C. English, "The Effect of Neutron Irradiation on Silicon Photodiodes," IEEE Trans. Nucl. Sci., Vol. 36, No. 6, pp. 2169-2175, 1989.

[LaBe93] K. A. LaBel, P. Marshall, C. Dale, C. M. Crabtree, E.G. Stassinopoulos, J. T. Miller and M. M. Gates, "SEDS MIL-STD-1773 Fiber Optic Data Bus: Proton Irradiation Test Results and Spaceflight SEU Data," IEEE Trans. Nucl. Sci., Vol. 40, No. 6, pp. 1638-1644, 1993.

[LaBe98] K.A. LaBel, A.H. Johnston, J.L. Barth, R.A. Reed, and C.E. Barnes, "Emerging Radiation Hardness Assurance (RHA) Issues: A NASA Approach for Spaceflight Programs," IEEE Trans. Nucl. Sci., Vol. 45, No. 6, pp. 2727-2736, 1998.

[Lang74] D.V. Lang and L.C. Kimerling, "Observations of Recombination-Enhanced Defect Reactions in Semiconductor," Phys. Rev. Lett., Vol. 33, No. 8, pp. 489-492, 1974.

[Lars78] B.C. Larsen, R.T. Young, and J. Narayan, "Defect Annealing Studies in Neutron Transmutation Doped Si," Neutron Transmutation Doping in Semiconductors, edited by J.M. Meese, Plenum Press, NY, pp. 781-290, 1978.

(All references are unclassified.)

[Lisc92] H. Lischka, H. Henschel, W. Lennartz, and H.U. Schmidt, "Radiation Sensitivity of Light Emitting Diodes (LED), Laser Diodes (LD) and Photodiodes (PD)," IEEE Trans. Nucl. Sci., Vol. 39, No. 3, pp. 423-427, 1992.

[Lisc93] H. Lischka, H. Henschel, O. Kohn, W. Lennartz, and H.U. Schmidt, "Radiation Effects in Light Emitting Diodes, Laser Diodes, Photodiodes, and Optocouplers," RADECS93, IEEE Doc. No. 93TH0616-3, pp. 226-231, 1993.

[Lisc94] H. Lischka, H. Henschel, O. Kohn, W. Lennartz, and H.U. Schmidt, "Radiation Effects in Optoelectronic Devices," Proc. SPIE, Vol. 2425, pp. 43-52, 1994.

[Lind63] J. Lindhard, V. Nielsen, M. Scharff, and P. Thomsen, "Integral Equations Governing Radiation Effects (Notes on Atomic Collisions, III)," Mat. Fys. Medd. Dan. Vid. Selsk., Vol. 33, No. 10, p.1, 1963.

[Luer87] T.F. Luera, J.G. Kelly, H.J. Stein, M.S. Lazo, C.E. Lee, and L.R. Dawson, "Neutron Damage Equivalence for Silicon, Silicon Dioxide, and Gallium Arsenide," IEEE Trans. Nucl. Sci., Vol. 34, No. 6, pp. 1557-1563, 1987.

[Mars89a] P.W. Marshall, C.J. Dale, G.P. Summers, E.A. Burke, and E.A. Wolicki, "Proton, Neutron and Electron Induced Displacement Damage in Germanium," IEEE Trans. Nucl. Sci., Vol. 36, pp. 1882-1888, 1989.

[Mars89b] P. W. Marshall, C. J. Dale, E. A. Burke, G. P. Summers, and G.E. Bender, "Displacement Damage Extremes in Silicon Depletion Regions," IEEE Trans. Nucl. Sci., Vol. 36, No. 6, pp. 1831-1839, 1989.

[Mars90] P.W. Marshall, C.J. Dale, E.A. Burke, "Proton-Induced Displacement Damage Distributions and Extremes in Silicon Microvolumes," IEEE Trans. Nucl. Sci., Vol. 37, No. 6, pp. 1776-1783, 1990.

[Mars92] P.W. Marshall, C.J. Dale, and E.A. Burke, "Space Radiation Effects on Optoelectronic Materials and Components for a 1300 nm Fiber Optic Data Bus," IEEE Trans. Nucl. Sci., Vol. 39, No. 6, pp. 1982-1989, 1992.

[Mars94] P.W. Marshall, C.J. Dale, K.A. LaBel, and E.J. Friebele, "A Review of Space Radiation Effects for Fiber Optic Data Links," SPIE Critical Review CR-14, Fiber Optics Reliability and Testing, 1994.

[Marv99] D.C. Marvin, J.C. Nocerino, and W.R. James, "Evaluation of Multijunction Solar Cell Performance in Radiation Environments," 1999 GOMAC Proc., pp. 430-433, 1999.

[McNu81] P.J. McNulty, G.E. Farrell, and W.P. Tucker, "Proton Induced Nuclear Reactions in Silicon," IEEE Trans. Nucl. Sci., Vol. 28, No. 6, pp. 4007-4012, 1981.

[McNu94] P.J. McNulty, W. G. Abdel-Kader, and G. E. Farrell, "Proton Induced Spallation Reactions," Radiat. Physi. Chem., Vol. 43 (1/2), pp. 139-149, 1994.

(All references are unclassified.)

[Mess86] G.C. Messenger and M.S. Ash, The Effect of Radiation on Electronic Systems, Van Nostrand Reinhold Company, NY, 1986, Chapter 5.

[Mess97a] S.R. Messenger, M.A. Zapsos, R.J. Walters, H.J. Cotal, S.J. Wojtczuk, H.B. Serreze, and G.P. Summers, "Spectral Response of InP/Si Solar Cells Irradiated to High Proton Fluences," Record of 26th IEEE Photovoltaic Specialists Conference, IEEE Catalog No. 97CB36026, pp. 815-818, 1997.

[Mess97b] S.R. Messenger, M.A. Xapsos, E.A. Burke, R.J. Walters, and G.P. Summers, "Proton Displacement Damage and Ionizing Dose for Shielded Devices in Space," IEEE Trans. Nucl. Sci., Vol. 44, No. 6, pp. 2169-2173, 1997.

[Mess98] S.R. Messenger, R.J. Walters, M.A. Xapsos, G.P. Summers, and E.A. Burke, "Carrier Removal in p-Type InP," IEEE Trans. Nucl. Sci., Vol. 45, No. 6, pp. 2857-2860, 1998.

[Mill94] T.L. Miller, D.A. Thompson, M.B. Elzinga, T.-H. Lee, B.C. Passenheim, and R.E. Leadon, "Experimental Evaluation of High Speed CCD Imager Radiation Effects Using Co60 and Proton Irradiation," 1993 IEEE Radiation Effects Data Workshop, pp. 56-63, 1994.

[Mind76] H.T. Minden, "Effects of Proton Bombardment on the Properties of GaAs Laser Diodes," J. Appl. Phys., Vol. 47, No. 3, pp. 1090-1094, 1976.

[Mohs74] A.M. Mohsen and M.F. Tompsett, "The Effects of Bulk Traps on the Performance of Bulk Channel Charge-Coupled Devices," IEEE Trans. Elect. Dev., Vol. 21, No. 11, pp. 701-711, 1974.

[More82] R.M. More and J.A. Spitznagel, "Primary Recoil Spectra and Subcascade Effects in Ion Bombardment Experiments," Rad. Eff., Vol. 60, pp. 27-33, 1982.

[Muel82] G.P. Mueller, N.D. Wilsey, and M. Rosen, "The Structure of Displacement Cascades in Silicon," IEEE Trans. Nucl. Sci., Vol. 29, No. 6, pp. 1293-1297, 1982.

[Nara81] J. Narayan and J. Fletcher, Defects in Semiconductors, edited by J. Narayan and P. Tan, North Holland, London, 1981.

[Niu98] G. Niu, G. Banerjee, J.D. Cressler, J.M. Roldan, S.D. Clark, and D.C. Ahlgren, "Electrical Probing of Surface and Bulk Traps in Proton-Irradiated Gate-Assisted Lateral PNP Transistors," IEEE Trans. Nucl. Sci., Vol. 45, No. 6, pp. 2361-2365, 1998.

[Nara88] Private communication with J. Narayan.

[Nogu90] T. Noguchi and M. Uesugi, "Electron Energy Dependence of Relative Damage Coefficients of Silicon Solar Cells for Space Use," Technical Digest of the International PVSEC-5, Kyoto, Japan, 1990.

(All references are unclassified.)

[Ohya96] H. Ohyama, J. Vanhellemont, Y. Takami, K. Hayama, T. Kudo, H. Sunaga, I. Hironaka, Y. Uwatoko, J. Poortmans, and M. Caymax, "Degradation and Recovery of Proton Irradiated $Si_{1-x}Ge_x$ Devices," IEEE Trans. Nucl Sci., Vol. 43, No. 6, pp. 3089-3096, 1996.

[Peas87] R.L. Pease, E.W. Enlow, G.L. Dinger, and P.W. Marshall, "Comparison of Neutron and Proton Carrier Removal Rates," IEEE Trans. Nucl. Sci., Vol. 34, No. 6, pp. 1140-1146, 1987.

[Pick93] J. Pickel, "Novel Devices and Sensors," IEEE Nuclear and Space Radiation Effects Conference Short Course Notes, Snowbird, UT, July 1993, pp. IV 1-60.

[Raym87] J.P. Raymond and E.L. Petersen, "Comparison of Neutron, Proton and Gamma Ray Effects in Semiconductor Devices," IEEE Trans. Nucl. Sci., Vol. 34, No. 6, pp. 1622-1628, 1987.

[Rax96] B.G. Rax, C.I. Lee, A.H. Johnston, and C.E. Barnes, "Total Dose and Proton Damage in Optocouplers," IEEE Trans. Nucl. Sci., Vol. 43, No. 6, pp. 3167-3173, 1996.

[Rax97] B.G. Rax, C.I. Lee, and A.H. Johnston, "Degradation of Precision Reference Devices in Space Environments," IEEE Trans. Nucl. Sci., Vol. 44, No. 6, pp.1939-1944, 1997.

[Rax98] B.G. Rax, A.H. Johnston, and C.I. Lee, "Proton Damage Effects in Linear Integrated Circuits," IEEE Trans. Nucl. Sci., Vol. 45, No. 6, pp. 2632-2637, 1998.

[Reed98] R.A. Reed, P.W. Marshall, A.H. Johnston, J.L. Barth, C.J. Marshall, K.A. LaBel, M. D'Ordine, H.S. Kim, and M.A. Carts, "Emerging Optocoupler Issues with Energetic Particle-Induced Transients and Permanent Radiation Degradation," IEEE Trans. Nucl. Sci., Vol. 45, No. 6, pp. 2833-2841, 1998.

[Robb92] M. Robbins, "Radiation Damage Effects in Charge Coupled Devices," Ph.D. Dissertation, Brunel University, 1992.

[Rold97] J.M. Roldan, W.E. Ansley, J.D. Cressler, S.D. Clark, and D. Nguyen-Ngoc, "Neutron Radiation Tolerance of Advanced UHV/CVD SiGe HBT BiCMOS Technology," IEEE Trans. Nucl. Sci., Vol. 44, No. 6, pp.1965-1973, 1997.

[Rold98] J.M. Roldan, G. Niu, W.E. Ansley, J.D. Cressler, S.D. Clark, and D.C. Ahlgren, "An Investigation of the Spatial Location of Proton-Induced Traps in SiGe HBTs," IEEE Trans. Nucl. Sci., Vol. 45, No. 6, pp. 2424-2429, 1998.

[Rose82] B.H. Rose and C.E. Barnes, "Proton Damage Effects on Light Emitting Devices," J. Appl. Phys., Vol. 53, No. 3, pp. 1772-1780, 1982.

[Sext92] F.W. Sexton, D.M. Fleetwood, C.C. Albridge, G. Garrett, J.C. Pelletier, and J.I. Gaona, "Qualifying Commercial ICs for Space Total-Dose Environments," IEEE Trans. Nucl. Sci., Vol. 39, No. 6, pp. 1869-1875, 1992.

(All references are unclassified.)

[Schr82] D.K. Schroder, "The Concept of Generation and Recombination Lifetimes in Semiconductors," IEEE Trans. Elect. Dev., Vol 29, No. 8, pp. 1336-1338, 1982.

[Soda75] K. Soda, C. Barnes and R. Kiehl, "The Effects of Gamma Irradiation on Optical Isolators," IEEE Trans. Nucl. Sci., Vol. 22, No. 6, p. 2475, 1975.

[Spra97] J.P. Spratt, B.C. Passenheim, and R.E. Leadon, "The Effects of Nuclear Radiation on P-Channel CCD Imagers," 1997 IEEE Radiation Effects Workshop Record, IEEE No. 97TH8293, pp. 116-121, 1997.

[Srou70] J.R. Srour, "Short-Term Annealing in Electron-Irradiated p-Type Silicon," IEEE Trans. Nucl. Sci., Vol. 17, No. 6, pp. 118-122, 1970.

[Srou79] J.R. Srour, S.C. Chen, S. Ottmer and R.A. Hartman, "Radiation Damage Coefficients for Silicon Depletion Regions," IEEE Trans. Nucl. Sci., Vol. 26, No. 6, pp. 4784-4791, 1979.

[Srou86] J.R. Srour, R.A. Hartman, and K.S. Kitazaki, "Permanent Damage Produced by Single Proton Interactions in Silicon Devices," IEEE Trans. Nucl. Sci., Vol. 33, No. 6, pp. 1597-1604, 1986.

[Srou88a] J.R. Srour, "Displacement Damage Effects in Electronic Materials, Devices, and Integrated Circuits," IEEE Nuclear and Space Radiation Effects Conference Short Course Notes, Portland, OR, July 1988, pp. IV 1-77.

[Srou88b] J.R. Srour and J.M. McGarrity, "Radiation Effects on Microelectronics," Proc. IEEE, Vol. 76, pp. 1443-1469, 1988.

[Srou89] J.R. Srour and R.A. Hartman, "Enhanced Displacement Damage Effectiveness in Irradiated Silicon Devices," IEEE Trans. Nucl. Sci., Vol. 36, No. 6, pp. 1825-1830, 1989.

[Srou98] J.R. Srour, G.J. Vendura, Jr., D.H. Lo, C.M.C. Toporow, M. Dooley, R.P. Nakano, and E.E. King, "Damage Mechanisms in Radiation-Tolerant Amorphous Silicon Solar Cells," IEEE Trans. Nucl. Sci., Vol. 45, No. 6, pp. 2624-2631, 1998.

[Summ87] G.P. Summers, C.J. Dale, E.A. Burke, E.A. Wolicki, P.W. Marshall, and M.A. Gehlhausen, "Correlation of Particle-Induced Displacement Damage in Silicon," IEEE Trans. Nucl. Sci., Vol. 34, pp. 1134-1139, 1987.

[Summ88] G.P. Summers, E.A. Burke, M.A. Xapsos, C.J. Dale, P.W. Marshall, and E.L. Petersen, "Displacement Damage in GaAs Structures," IEEE Trans. Nucl. Sci., Vol. 35, No. 6, p. 1221, 1988.

[Summ92] G.P. Summers, "Displacement Damage: Mechanisms and Measurements," IEEE Nuclear and Space Radiation Effects Conference Short Course Notes, New Orleans, LA, July 1992, pp. IV 1-58.

(All references are unclassified.)

[Summ93] G.P. Summers, E.A. Burke, P. Shapiro, S.R. Messenger, and R. J. Walters, "Damage Correlations in Semiconductors Exposed to Gamma, Electron and Proton Radiations," IEEE Trans. Nucl. Sci., Vol. 40, No. 6, pp. 1372-1379, 1993.

[Summ94] G.P. Summers, R.J. Walters, M.A. Xapsos, E.A. Burke, S.R. Messenger, P. Shapiro and R.L. Statler, "A New Approach to Damage Prediction for Solar Cells Exposed to Different Radiations," Record of 24th IEEE Photovoltaic Specialists Conferences, IEEE Catalog No. 94CH3365-4, pp. 2068-2075, 1994.

[Sun97] X. Sun, D. Reusser, H. Dautet, and J.B. Abshire, "Measurement of Proton Radiation Damage to Si Avalanche Photodiodes," IEEE Trans. Elect. Dev., Vol. 44, No. 12, pp. 2160-2166, 1997.

[Sun99] Proton irradiated avalanche photodiodes have exhibited significant room temperature annealing. Private communication with X. Sun.

[Tada82] H.Y. Tada, J.R. Carter, B.E. Anspaugh, R.G. Downing, Solar Cell Radiation Handbook, JPL Publication 82-69, 1982.

[VanL80] V.A.J. van Lint, T.M. Flanagan, R.E. Leadon, J.A. Naber, and V.C. Rogers, Mechanisms of Radiation Effects in Electronic Materials, Volume 1, John Wiley and Sons, NY, 1980.

[VanG89] A. Van Ginneken, "Non-Ionizing Energy Deposition in Silicon for Radiation Damage Studies," Fermi National Accelerator Laboratory, P.O. Box 500, Batavia, IL 60510, Batavia FN-522, October 1989.

[Walk73] J.W. Walker and C.T. Sah, "Properties of 1.0 MeV Electron-Irradiated Defect Centers in Silicon," Phys. Rev. B, Vol. 7, No. 10, p. 4587-4605, 1973.

[Walt91] R.J. Walters, S.R. Messenger, G.P. Summers, E.A. Burke, and C.J. Keavney, "Space Radiation Effects in InP Solar Cells," IEEE Trans. Nucl. Sci., Vol. 38, No. 6, pp. 1153-1158, 1991.

[Walt99] R.J. Walters, M.A. Xapsos, G.P. Summers, and S.R. Messenger, "Analysis and Modeling of the Radiation Response of Space Solar Cells," 1999 GOMAC Proc., pp. 434-437, 1999.

[Wate87] J.R. Waterman and R.A. Schiebel, "Ionizing Radiation Effects in n-Channel HgCdTe MISFET's with Anodic Sulphide Passivation," IEEE Trans. Nucl. Sci., Vol. 34, No. 6, pp. 1597-1601, 1987.

[Watk64] G.D. Watkins and J.W. Corbett, "Defects in Irradiated Silicon: Electron Paramagnetic Resonance and Electron-Nuclear Double Resonance of the Si-E Center," Phys. Rev., Vol. 134, No. 5A, pp. 1359-1377, 1964.

[Wicz82] J. Wiczer, L. Dawson, G. Osburn and C. Barnes, "Permanent Damage Effects in Si and AlGaAs/GaAs Photodiodes," IEEE Trans. Nucl. Sci., Vol. 29, No. 6, pp. 1539-1544, 1982.

(All references are unclassified.)

[Wood81] S. Wood, N.J. Doyle, J.A. Spitznagel, W.J. Choyke, R.M. More, J.N. McGruer, and R.B. Irwin, "Simulation of Radiation Damage in Solids," IEEE Trans. Nucl. Sci., Vol. 28, pp. 4107-4122, 1981.

[Yama84] M. Yamaguchi, C. Uemura, and A. Yamamoto, "Radiation Damage in InP Single Crystals and Solar Cells," J. Appl. Phys., Vol. 55, pp. 1429-1436, 1984.

[Yama88] M. Yamaguchi and K. Ando, "Mechanism for Radiation Resistance in InP Solar Cells," J. Appl. Phys., Vol. 63, p. 5555, 1988.

[Yama96] M. Yamaguchi, S.J. Taylor, M. Yang, S. Matsuda, O. Kawasaki, and T. Hisamatsu, "High-Energy and High-Fluence Proton Irradiation Effects in Silicon Solar Cells," J. Appl. Phys., Vol. 80, pp. 4916-4920, 1996.

[Zeig84] J.F. Zeigler, J.P. Biersack, and U. Littmark, The Stopping and Range of Ions in Solids, Pergamon Press, New York, 1984.

[Zhao97] Y.F. Zhao, A.R. Patwary, R.D. Schrimpf, M.A. Neifeld, and K.F. Galloway, "200 MeV Proton Damage Effects on Multi-Quantum Well Laser Diodes," IEEE Trans. Nucl. Sci., Vol. 44, pp. 1898-1905, 1997.

[Zhao98] Y.F. Zhao, R.D. Schrimpf, A.R. Patwary, M.A. Neifeld, A.W. Al-Johani, R.A. Weller, and K.F. Galloway, "Annealing Effects on Multi-Quantum Well Laser Diodes after Proton Irradiation," IEEE Trans. Nucl. Sci., Vol. 44, pp. 2826-2832, 1997.